The Influence of Layer Outcropping on the Separation of Boundary Currents. Part I: The Wind-driven Experiments

ERIC P. CHASSIGNET AND RAINER BLECK

RSMAS/MPO, University of Miami, Miami, Florida

(Manuscript received 30 January 1992, in final form 23 September 1992)

ABSTRACT

The influence of outcropping isopycnal layers on the separation of western boundary currents is investigated in a series of wind-driven eddy-resolving multilayer primitive equation numerical experiments. The outcropping mechanism of Parsons allows the midlatitude jet to separate south of the zero wind-stress curl line (ZWCL), an important property when one considers that most realistic numerical experiments to date exhibit an overshooting subtropical western boundary current.

If the inertial terms are removed from the momentum equations, the Sverdrup relation for the interior flow emerges as the dominant constraint on the placement of the upper-layer jet separation latitude. As long as the upper/lower layer ratio is small enough, a good agreement is obtained with the analytical theory, namely a separation south of the ZWCL. If the ratio is large, the resulting flow pattern changes drastically by favoring a configuration that satisfies the Sverdrup relation and maintains a jet separation at the ZWCL.

As soon as the inertial terms are included, the Sverdrup constraint becomes less dominant, allowing the upper-layer midlatitude jet separation latitude to shift southward whenever the upper layer is chosen sufficiently shallow to cause large-scale outcropping. The degree to which this southward shift depends on the amount of mass in the top layer and on the parameterization of the wind-induced stress profile in the water column is explored in detail.

1. Introduction

The earliest models of the wind-driven ocean circulation in a closed basin [see Veronis (1981) for a review] were based on the linearized, steady-state, shallow-water equations with simple closure schemes for frictional dissipation. These models represented the flow in an active surface layer of essentially constant depth above a deep layer at rest. Welander (1966) generalized this model by allowing large upper-layer depth variations but retained the linearized form of the momentum equations. Parsons (1969) extended Welander's model by permitting depth variations large enough for outcropping to occur. The outcropping mechanism in his solution provides one of the simplest explanations of separation of the western boundary current in subtropical gyres and has been applied by Kamenkovich and Reznik (1972), Veronis (1973), Moore and Niiler (1974), Anderson and Moore (1979), Ou and de Ruijter (1986), Huang (1984, 1986, 1987), and Huang and Flierl (1987). Veronis (1981) in his review paper summarizes the preceding viewpoint by stating

> ". . . the present analysis suggests that an explanation of the separation of western boundary currents from the coast must necessarily include the surfacing of the thermocline (with a possible mixed layer at the surface). Western boundary currents can be forced out to sea between wind-driven gyres of opposite signs, but that occurs at low latitudes as well where the phenomenon is qualitatively different because the thermocline does not surface."

The latter description applies to the separation mechanism of numerical solutions such as those of Bryan (1963), Holland and Lin (1975), Holland (1978), Bleck and Boudra (1981, 1986), McWilliams et al. (1990), Haidvogel et al. (1991), and others which depends strongly on inertial effects in the equations of motion since the thermocline does not outcrop [see Ierley (1990) for a review].

As stated by Huang (1987), theoreticians favor layered models because of their conceptual simplicity, while numerical modelers tend to use geometric vertical coordinates. As a result, a significant gap has developed between traditional numerical and analytical models, which could effectively be reduced with the use of layered models. Until recently, numerical investigation of regimes with layer outcropping has been inhibited because of the numerical difficulty induced by moving layers intersecting the ocean surface. Bogue et al. (1986) performed the first series of numerical experiments de-

Corresponding author address: Dr. Eric P. Chassignet, RSMAS, University of Miami, Division of Meteorology and Phys. Ocean, 4600 Rickenbacker Causeway, Miami, FL 33149-1098.

signed to reproduce the solutions given by Parsons (1969) for the linearized shallow-water equations. In particular, they were interested in qualitative comparisons in the region where the layer interface intersects the sea surface and quantitative comparisons in the basin interior. Good agreement was obtained. They successfully used, as did Bleck and Boudra (1986) and Huang (1986, 1987), the flux-corrected transport (FCT) algorithm of Boris and Book (1973), generalized by Zalesak (1979). In his coarse-resolution multilayer numerical model simulation of a subtropical–subpolar basin, Huang (1987) was able to represent the very large-scale features of the ocean circulation. For certain parameter settings, the model produced boundary currents looping around the edge of an outcropping zone that resemble the current system of the North Atlantic.

The possible importance of outcropping on Gulf Stream separation is illustrated in the purely wind-driven North Atlantic simulation of Smith et al. (1990) performed with a non–eddy resolving version of the Bleck and Boudra (1986) numerical model. To our knowledge, most existing realistic North Atlantic experiments exhibit an overshooting Gulf Stream (Thompson and Schmitz 1989). In contrast to this, Smith et al. (1990) found that their western boundary current separated from the coast near Cape Hatteras, that is, at approximately the correct latitude. The first model interface was observed to outcrop along the fringe of the subtropical gyre and it is surmised that the initial choice of upper-layer thickness (effectively the total amount of model Sargasso Sea water) may have played a role in obtaining a correct separation.

The horizontal resolution used in both Huang (1987) and Smith et al. (1990) limited the model's ability to resolve frontal features such as midlatitude jets and eddies. Only by extending model calculations to the eddy-resolving scale can we study these features. In this paper, we describe a series of purely wind-driven eddy-resolving primitive equation numerical experiments of increasing complexity designed to investigate the separation mechanism of the midlatitude jet in the presence of layer outcropping.

If the inertial terms are removed from the momentum equations, the Sverdrup relation for the interior flow emerges as the dominant constraint on the placement of the upper-layer jet separation latitude. Discrepancies between Huang's (1984) analytic solutions, some of which show a separation point far to the south of the zero wind-stress curl line (ZWCL), and Huang's (1987) numerical solutions showing a jet separating at the ZWCL will be traced to the fact that in some steady-state analytical solution, steepening of the front is not allowed.

As soon as the inertial terms are included, the Sverdrup constraint becomes less dominant, allowing the upper-layer midlatitude jet separation latitude to shift southward whenever the upper layer is chosen sufficiently shallow to cause large-scale outcropping. We will explore the degree to which this southward shift depends on the amount of mass in the top layer and on the parameterization of the wind-induced stress profile in the water column.

The layout of the paper is the following. First, section 2 presents the numerical model characteristics and parameters. In section 3, previous relevant analytical and numerical studies are reviewed. The multilayer noninertial experiments and the constraint due to the Sverdrup relation are discussed in detail in section 4. Section 5 then presents the impact of the inertial terms on the midlatitude jet separation. Finally, the results are summarized and discussed in the concluding section.

2. The numerical model

The primitive equation, pure-isopycnic model of Bleck and Boudra (1986) may be viewed as a stack of shallow-water models, each consisting of a momentum and a continuity equation:

$$\frac{\partial \mathbf{v}}{\partial t} + \frac{1}{2}\nabla_\rho \mathbf{v}^2 + (\zeta + f)\mathbf{k} \times \mathbf{v} = -\nabla_\rho M + \alpha \frac{\partial \boldsymbol{\tau}}{\partial z} + Ah^{-1}\nabla_\rho \cdot h\nabla\rho\mathbf{v} - \sigma\mathbf{v}, \quad (1)$$

$$\frac{\partial h}{\partial t_\rho} + \nabla_\rho \cdot (\mathbf{v}h) = 0, \quad (2)$$

where $\zeta = v_x - u_y$ is the vorticity; $M = gz + p\alpha$ is the Montgomery potential; h is the thickness of a layer of constant density; $\alpha = \rho^{-1}$ is the specific volume; $\boldsymbol{\tau}$ is the wind stress; A is the lateral viscosity; and the bottom drag coefficient σ is zero except in the bottom layer. The subscript ρ indicates derivatives on surfaces of constant density. The shallow-water models communicate vertically through hydrostatically transmitted pressure forces. Horizontal velocities and vorticity are defined as layer properties while pressure and geopotential are defined at the interfaces between layers.

One of the primary difficulties of layered models is the intersection of the moving coordinate surfaces with boundaries, such as the sea surface (outcropping). This problem has in general been sidestepped in previous studies by choosing a sufficiently thick upper layer (Holland and Lin 1975; Thompson and Schmitz 1989) or by the use of hybrid coordinates (Bleck and Boudra 1981). The adoption of a special algorithm, the FCT algorithm (Boris and Book 1973; Zalesak 1979), which combines the smoothness properties of the positive-definite upstream differencing scheme with the accuracy of space-centered schemes, controls the tendency to generate negative layer thickness when solving the layer thickness prediction equation. This approach has proven very effective (Bleck and Boudra 1986; Bogue et al. 1986; Huang 1986, 1987; Huang and Bryan 1987; Bleck and Smith 1990).

The model is configured for this study in a square ocean basin (2000 km × 2000 km × 5 km) driven by a zonally symmetric wind stress

$$\boldsymbol{\tau} = \left[-\tau_m \cos\left(\frac{2\pi y}{L}\right), 0\right],$$

where $\tau_m/\rho = 1 \times 10^{-4}$ m^2 s^{-2} specified as a body force acting only on the layer directly beneath the surface (Chassignet and Gent 1991). The horizontal grid is uniform with a spacing of 20 km. In the vertical, the initial spacing (4–6 layers) is nonuniform, with greater resolution near the surface. The resulting Sverdrup-gyre circulation is antisymmetric about midlatitude with a counterclockwise gyre north of the wind-stress curl zero and a clockwise gyre to the south. The circulation is damped by both a linear bottom drag and the minimum lateral eddy viscosity of the Laplacian form required for numerical stability. The lateral boundary conditions employed on the four sidewalls are free slip. In this paper, the only parameters changing from one experiment to the other are the eddy viscosity, the number of layers, their thicknesses, and corresponding densities. These changes are made such that the first two internal Rossby radii of deformation (when applicable) remain approximately constant (~30 and 15 km, respectively). The outcrop region is gradually increased and the influence on the jet separation and general circulation assessed. The parameters for the experiments are given in Table 1.

TABLE 1. Parameters of the experiments. For all experiments the linear bottom drag is 10^{-7} s^{-1}.

Experiment	Number of layers	Initial layer thickness (m)	g′ (m s^{-2})	Lateral dissipation (m^2 s^{-1})	λ
(N)I1	4	300	0.012	100	0.19
		400	0.004		
		800	0.004		
		3500			
(N)I2	4	150	0.014	200	0.65
		550	0.004		
		800	0.004		
		3500			
(N)I3	6	50	0.004	400	20.4
		50	0.004		
		200	0.004		
		400	0.004		
		800	0.004		
		3500			
NI4	2	150	0.06	200	0.15
		4850			
NI5	2	150	0.06	200	0.15
		550			

3. Review of previous analytical and numerical studies

Huang (1984) and Huang and Flierl (1987) extended the analytic models of Parsons (1969), Kamenkovich and Reznik (1972), and Veronis (1973) by including dynamics in the boundary layers. The flow pattern of a two-gyre basin in the case of an active layer overlying an infinitely deep quiescent layer is controlled by a single nondimensional number $\lambda = \tau_m L/g'H_1^2$, where τ_m is the maximum wind stress; L the basin width; g' the reduced gravity, and H_1 the mean upper-layer thickness. An increase in λ can then be related to either an increase in wind stress or a decrease in upper-layer mass. The nonlinearity associated with layer depth changes is included in these studies, but the inertial terms in the momentum equations are omitted. Huang (1984) distinguishes two regimes in the case of a single active layer: a subcritical one in the absence of outcropping and a supercritical one with outcropping. The latter can itself be divided into two subregimes: supercritical (I) in which the upper-layer thickness along the eastern wall is nonzero and supercritical (II) for a zero layer thickness. A third regime was introduced by Huang (1987) for multilayer cases: a hypercritical one where two or more layers outcrop.

In the case of one active layer (Fig. 1), the separation latitude and outcropping line move south as λ increases until reaching the supercritical (II) state (Huang 1984; Huang and Flierl 1987). The separation latitude then remains constant at the zero-wind line while the outcrop area keeps increasing with zero layer thickness along the eastern wall. These analytic results were reproduced numerically by Huang (1986). In the case of a finite second layer, Huang (1984) showed analytically that the upper-layer flow patterns remain similar to those for one active layer (Fig. 2). The second layer is then directly forced in the outcrop region by the wind stress and the circulation is such that the Sverdrup mass flux is zero at the ZWCL. Friction was represented by a vertical diffusion term with a constant eddy viscosity; a λ value higher than in the one-layer case was then required for the same outcrop area (Figs. 1 and 2).

4. The noninertial case

However, Huang's (1984) prediction of a southward movement of the separation latitude and outcropping line for either an increase in wind forcing or a decrease in upper-layer fluid volume was not confirmed by his multilayer numerical experiments (Huang 1987); the separation latitude always remained near the ZWCL. To investigate this discrepancy, we have carried out three multilayer experiments NI1, NI2, and NI3 with increasing outcrop region (λ = 0.19, 0.65, and 20.4, respectively) (Table 1). Layer thicknesses were chosen such that the first two internal Rossby radii of deformation remain approximately constant (~30 and 15 km, respectively). As in Huang (1984, 1987), the nonlinearity associated with layer depth changes was included while the inertial terms in the momentum

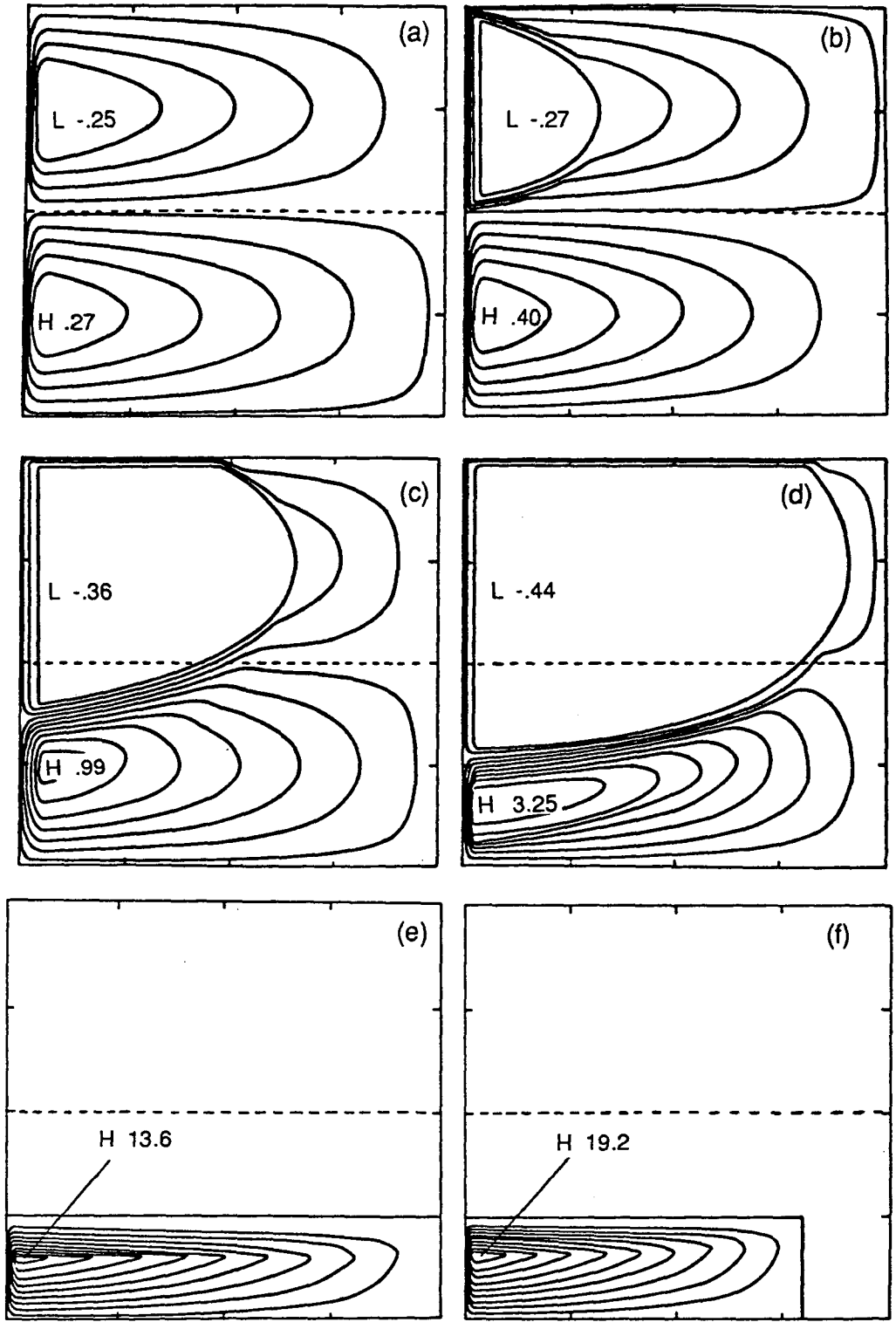

FIG. 1. Flow patterns for the one-layer analytical theory [after Huang (1984)]: (a) $\lambda = 0.047$, (b) 0.070, (c) 0.153, (d) 0.610, (e) 2.627, and (f) 5.130, where $\lambda = L\tau_m/g'H_1^2$.

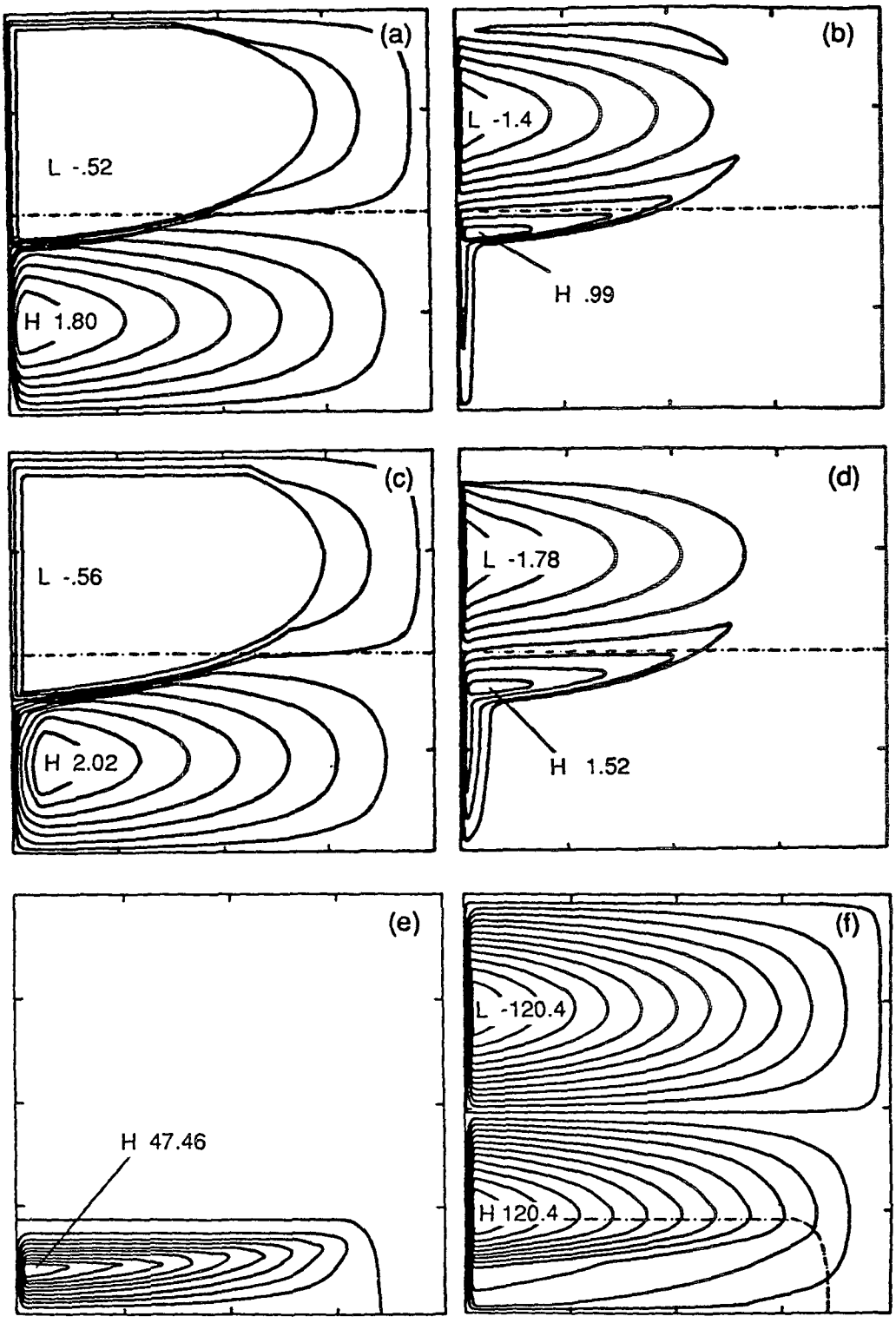

FIG. 2. Flow patterns for the two-layer analytical theory [after Huang (1984)]: (a, b) $\lambda = 0.3$, $\delta = 0.1$, $\epsilon = 0.03$; (c, d) 0.35, 0.04, 0.07; and (e, f) unknown, where $\lambda = L\tau_m/g'H_1^2$, $\delta = H_1/H_2$, and $\epsilon = (2A/f)^{1/2}/H_1$.

equations were omitted. The major difference with Huang's (1987) multilayer experiments is a finite-depth bottom layer.

a. *Description of the experiments*

The time averaged upper-layer thicknesses and streamfunctions of NI1, NI2, and NI3 are presented in Fig. 3. As the amount of upper-layer fluid is reduced from NI1 to NI3 (Table 1), the outcrop region increases in size to the point where it occupies half the domain in NI3. In both NI1 and NI2, the initial stratification is such that only one layer outcrops. In NI3, three out of six layers outcrop. This is illustrated by two meridional vertical cross-sections drawn at 100 and 700 km east of the western boundary (Fig. 4). As observed from both Fig. 3 and 4, the outcropping line does not cross the ZWCL (except in the eastern side of the domain for NI3) and the midlatitude jet always separates at the ZWCL. The outcropping line was also observed to remain near the ZWCL in the multilayer experiments of Huang (1987), and it can therefore be concluded that, in the absence of inertial terms in the momentum equations, the inclusion of a finite-depth bottom layer does not significantly modify the model's response. In all three experiments, the circulation (not illustrated) below the outcropping layers and above the bottom layer exhibits the classic two-gyre pattern with a more intense subpolar gyre underneath the outcrop region. A small countercirculation develops near the western boundary in the bottom layer indicating that the solutions did not reach an entirely steady state.

b. *On the constraints imposed by the Sverdrup relation*

At this point, one needs to investigate numerically the analytical results of Huang (1984) for a finite-depth lower layer (Fig. 2) since they differ from the multilayer experiments of section 4a and Huang (1987). The analytical development of Huang (1984) requires a small ratio $\delta = H_1/H_2$, and NI4 is therefore a two-layer experiment with a relatively thin upper layer and thick lower layer ($\delta = 1/30$, $\lambda = 0.15$) (Table 1). The nondimensional parameter λ is chosen here to obtain a large outcrop region and to keep the initial Rossby radius of deformation at approximately 30 km (Table 1). As in the previous experiments NI1, NI2, and NI3, the nonlinearity associated with layer depth changes is included, and the inertial terms in the momentum equations are omitted.

The solution reaches a steady state in which the upper-layer thickness and streamfunctions for the upper and lower layers of NI4 are as shown in Fig. 5. The outcrop area is seen to expand significantly south of the ZWCL (Fig. 5a) and the flow patterns in each layer (Figs. 5b,c) are in satisfactory agreement with the analytical results of Figs. 2c,d. The upper- and lower-layer flows are such that the meridional mass flux V across the ZWCL is close to zero and therefore satisfies the Sverdrup relation $\beta V = \text{curl } \boldsymbol{\tau}$ despite the presence of frictional effects in the model. The nondimensional number λ of the analytical solutions corresponding to Fig. 2c,d is slightly higher than for NI4, but one has to keep in mind that such a discrepancy was already noted between the one-layer and two-layer analytical theories (section 3). On the other hand, the upper-layer flow pattern (Fig. 5b) is in excellent agreement with the prediction of the single active layer theory (Fig. 1c). We attribute the differences to the various choices made in the parameterization of frictional processes in the analytical theories and in the numerical model.

The question then arises as to which factors are responsible for the difference in behavior between NI4 on the one hand, and NI1, NI2, NI3, and Huang (1987) on the other. The major difference is the number of layers and their thickness ratios. In NI4, the dominant feature is the baroclinic meridional exchange of mass consisting of southwestward flow in the lower layer underneath the northeastward upper-layer jet associated with the outcrop (Fig. 5). The flow reversal in the lower layer is needed to yield zero mass flux across the ZWCL as required by the Sverdrup relation.

This flow configuration is likely to change if the vertical shear between the two layers is increased, which will happen on account of the Sverdrup constraint if the upper/lower layer thickness ratio is decreased. If one considers a relatively thick lower layer with small velocities and large interface displacement, the presence of motion in the lower layer will affect the dynamics of the upper layer if $H_2 < f_0 H_1/\beta L$ (Chassignet and Cushman-Roisin 1991). For an upper-layer thickness of 150 m as in NI4 and a midlatitude jet width of 200 km, the criterion gives $\delta = H_1/H_2 > 1/25$. This is unlikely to be the case for NI4 since $\delta = 1/30$ and for Huang (1984) where a small ratio δ was required for the analytical development of his solution.

To investigate the importance of the upper/lower layer thickness ratio on the model's response, a two-layer experiment NI5, identical to NI4 except for a change in δ, was therefore performed. The layer ratio was chosen to represent the upper stratification of NI2 ($\delta = 1/4$) (Table 1). The time-averaged upper-layer thickness and streamfunctions for the upper and lower layers of NI5 are displayed in Fig. 6. In this experiment as in NI1, NI2, NI3, and the experiments of Huang (1987), the outcropping line does not cross the ZWCL (Fig. 6a) and the midlatitude jet separates at the ZWCL (Fig. 6b). As in NI4, the Sverdrup relation is satisfied in the interior, but with no baroclinic exchange of mass across the ZWCL. The solution reached a quasi steady state (Fig. 6c).

As already mentioned, in the case of a flow configuration that satisfies the Sverdrup relation as vertically aligned opposing currents as in NI4, the vertical shear between the two layers will increase for an increase in

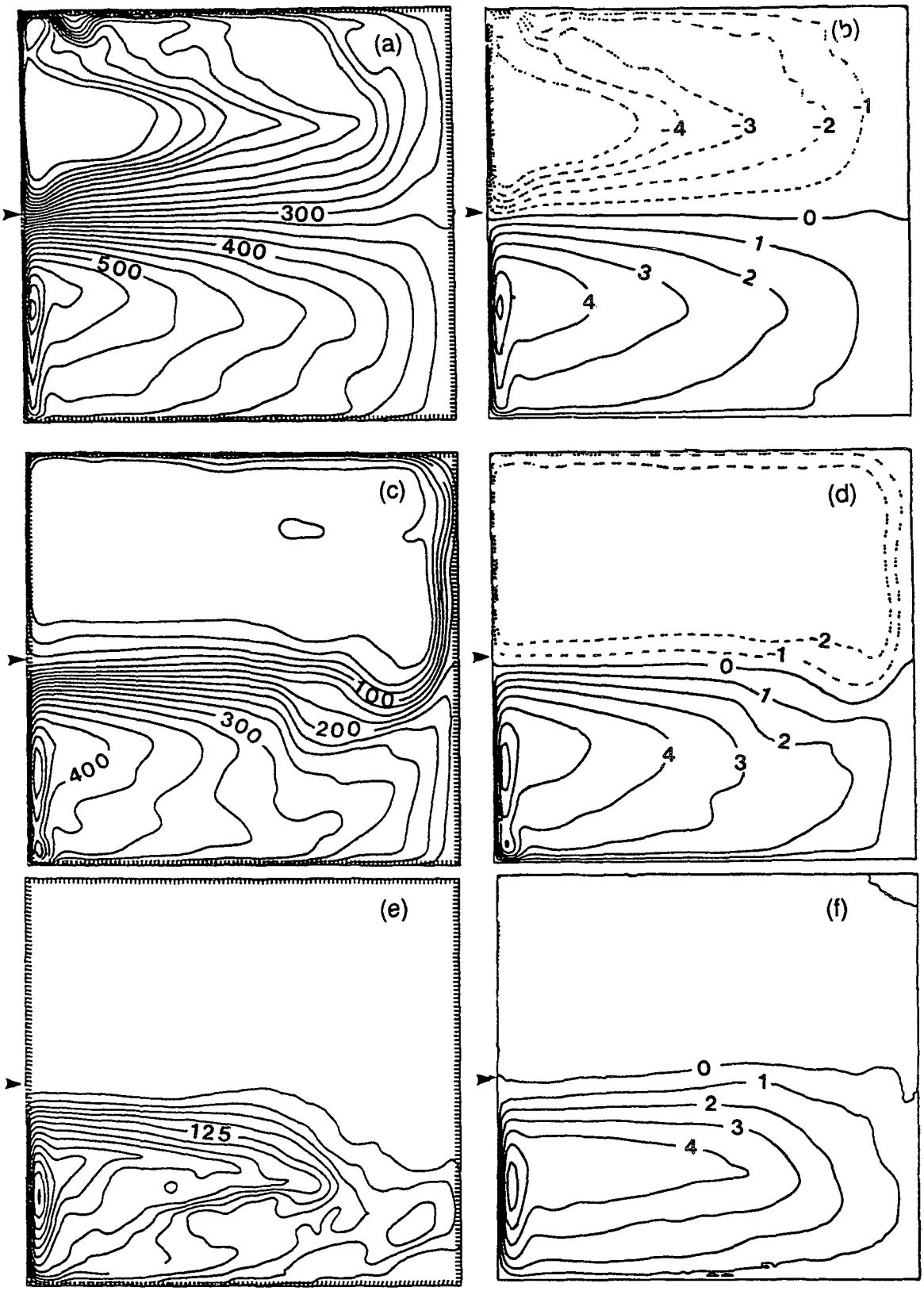

FIG. 3. Five-year time averages of the upper-layer thickness fields and velocity streamfunctions for NI1, NI2, and NI3, respectively. (a, c, e) The contour interval is 25 meters; (b, d, f) the contour interval is 10^4 m^2 s^{-1} and straddles zero symmetrically. The arrow indicates the ZWCL.

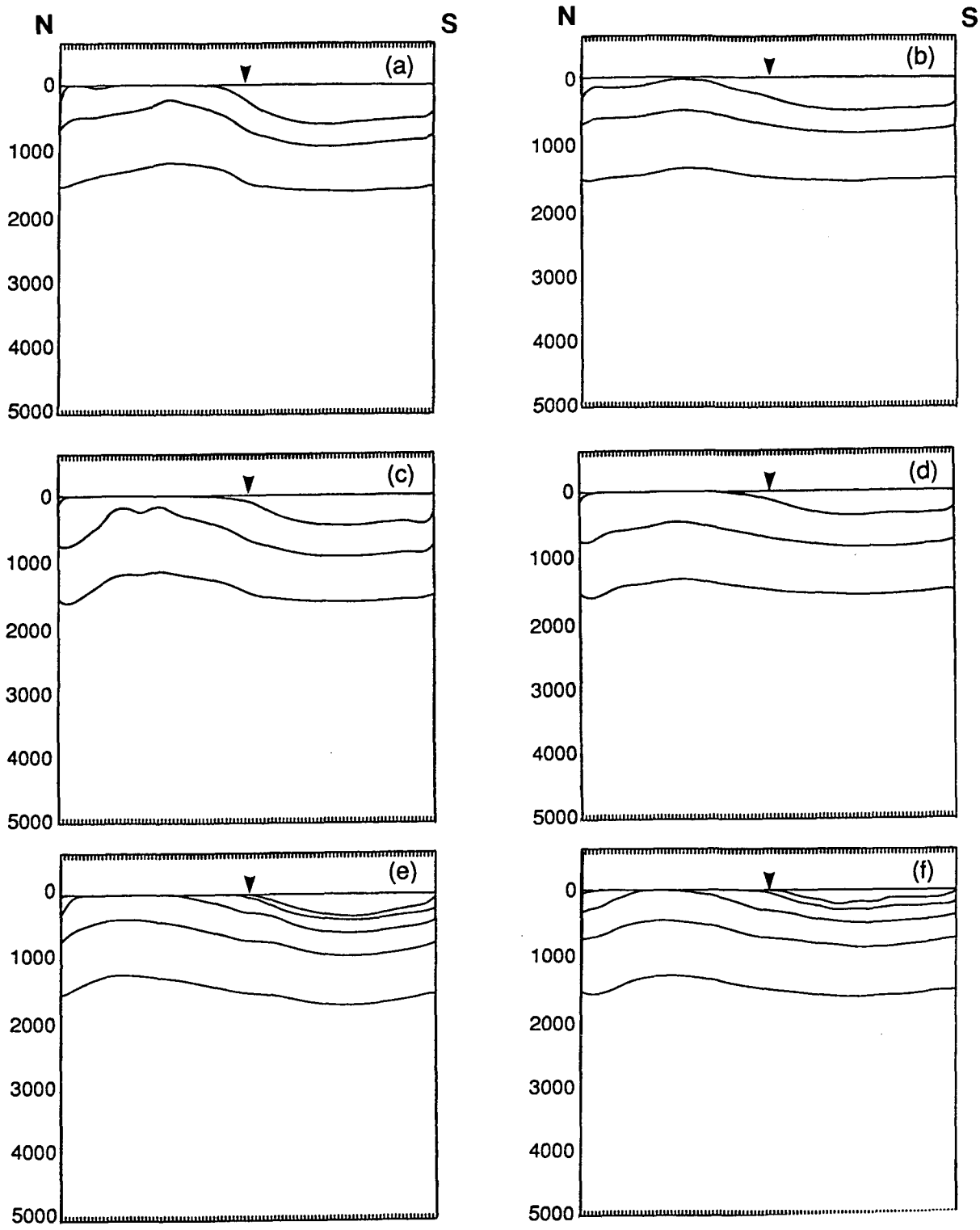

FIG. 4. Meridional vertical cross sections for NI1, NI2, and NI3 drawn at 100 km (a, c, e) and 700 km (b, d, f) east of the western boundary, respectively. The arrow indicates the ZWCL.

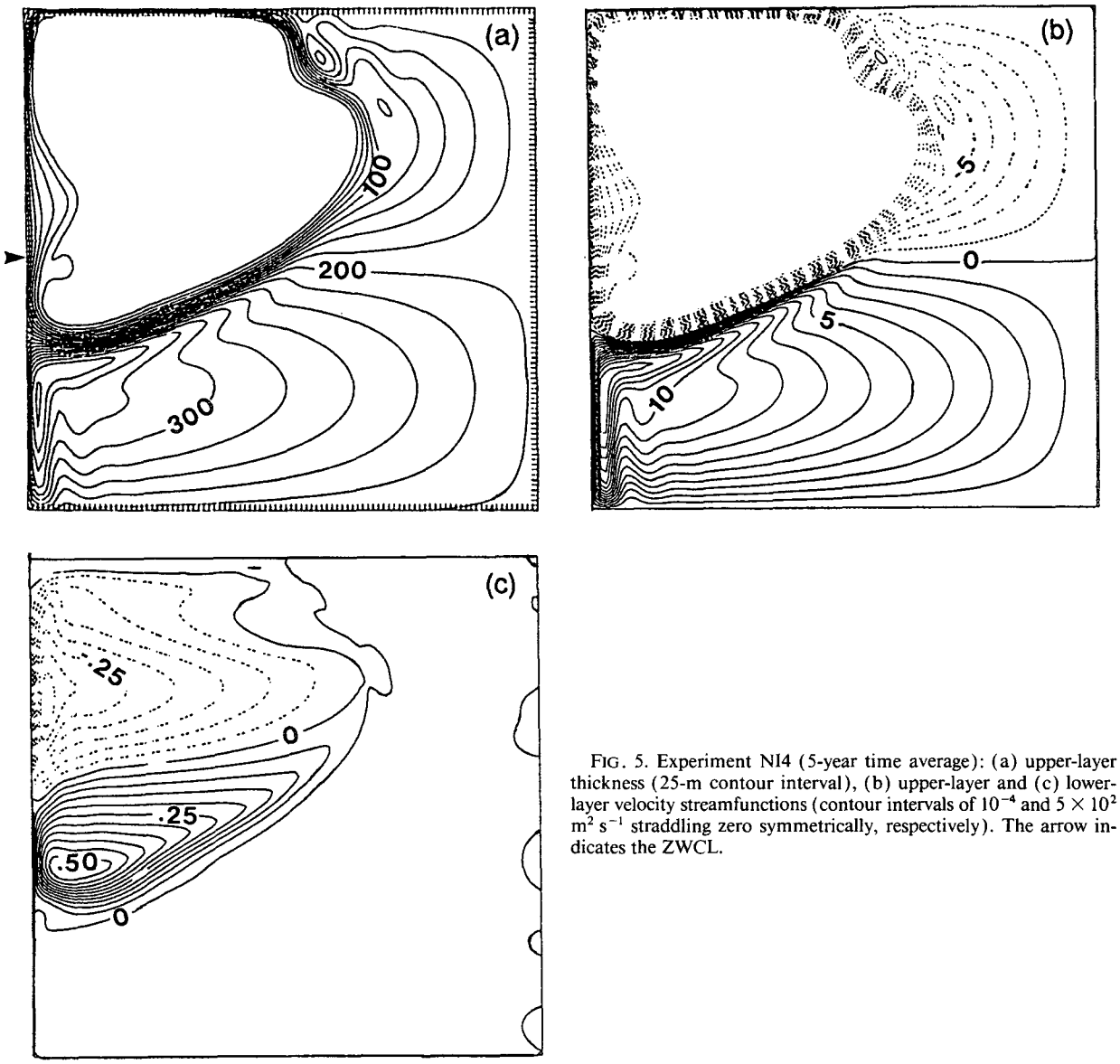

FIG. 5. Experiment NI4 (5-year time average): (a) upper-layer thickness (25-m contour interval), (b) upper-layer and (c) lower-layer velocity streamfunctions (contour intervals of 10^{-4} and 5×10^{2} $m^2\ s^{-1}$ straddling zero symmetrically, respectively). The arrow indicates the ZWCL.

the upper/lower layer ratio δ. One could therefore expect this situation to become baroclinically unstable (Phillips 1954; Pedlosky 1987a), were it not for the fact that the two-layer system is stable when the nonlinear terms are removed from the momentum equations. Baroclinic instability is not necessarily excised by the absence of inertial terms in the momentum equations, but more than two layers are needed (Colin de Verdière 1986). The question then arises as to why NI5 does not exhibit any opposing baroclinic mass fluxes across the ZWCL. This can be addressed using the theory of arrested fronts (Dewar 1991).

The two-layer formulation characterizing NI4 and NI5 [no inertial terms in (1)] can be reduced to one equation with one unknown, the upper-layer thickness h, by assuming the velocities to be in thermal wind balance (Anderson and Killworth 1979; Rhines 1986; Dewar 1987, 1991):

$$\frac{\partial h}{\partial t} - a\left(1 - \frac{h}{H}\right)h\frac{\partial h}{\partial x} = -\mathbf{V}_B \cdot \nabla h - \left(1 - \frac{h}{H}\right)\nabla \times \frac{\boldsymbol{\tau}}{f}, \quad (3)$$

where H is the total depth of the fluid, $a = \beta g'/f^2$, and $\mathbf{V}_B$ is the vertically averaged velocity such that $\nabla \cdot \mathbf{V}_B = (\nabla \times \boldsymbol{\tau}/f)/H$. As discussed by Rhines (1986) and Dewar (1987, 1991), the time dependence of (3) is that of a nonlinearly steepening Rossby wave, which leads to the formation of an outcropping front. The propagation of this wave is governed by the characteristics

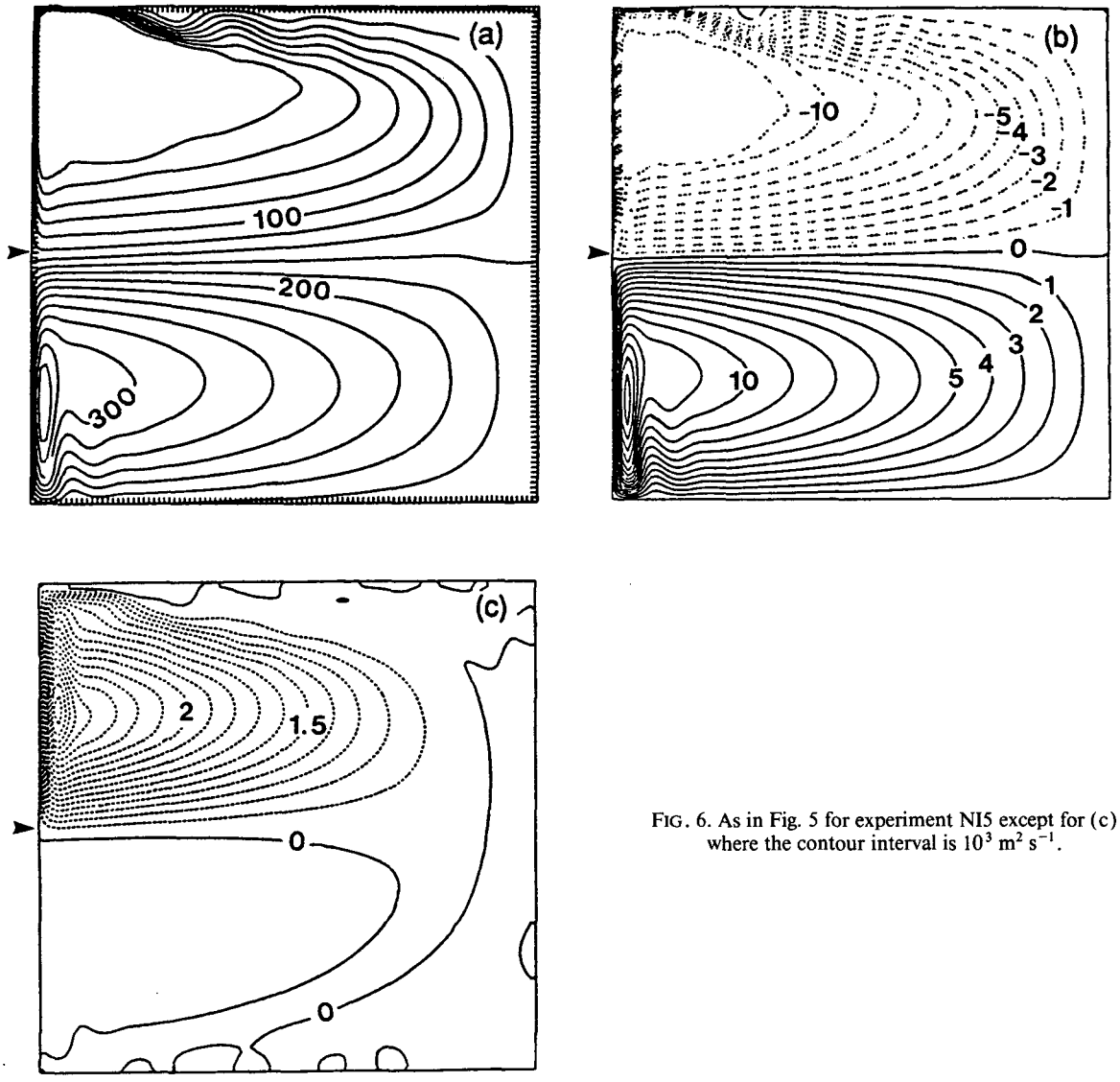

FIG. 6. As in Fig. 5 for experiment NI5 except for (c) where the contour interval is 10^3 m^2 s^{-1}.

$$\frac{\partial x}{\partial t} = U_B - ah\left(1 - \frac{h}{H}\right), \quad \frac{\partial y}{\partial t} = V_B \qquad (4)$$

and is westward unless the barotropic flow U_B is eastward and strong enough to stop the steepening (Rhines 1986). At the ZWCL, the vertically integrated velocity U_B is equal to $4\pi^2(L - x)\tau_m/\beta HL^2$. For NI4, H is large and U_B is therefore small enough to allow for westward propagation and steepening. On the other hand, in NI5, H is small, U_B is almost everywhere dominant, and there is no steepening of the wave leading to the formation of an outcrop on the ZWCL. Outcropping then occurs only when U_B is small or westward, namely, in the upper part of the domain (Fig. 6a).

It can then be concluded that, for the two-layer experiments in the absence of inertial terms in the momentum equations, the position of the outcropping line is dependent upon the value of the upper/lower layer thickness ratio δ. A scaling analysis of (4) leads to the following criterion. If $\delta < \delta_c = \beta^2 Lg'H_1^2/4\pi^2 f^2 \tau_m$, the outcropping line is south of the ZWCL in accordance with the analytical theory. The Sverdrup relation is satisfied in the interior. If $\delta > \delta_c$, the flow pattern changes drastically and the midlatitude jet separates at the ZWCL. The numerical solution then favors a flow configuration that satisfies the Sverdrup relation without requiring vertically aligned opposing currents, that is, no buildup of a baroclinic exchange of mass across the ZWCL. When applied to NI4 and NI5, δ_c is equal to 1/35 and is in agreement with the preceding findings. The criterion has been derived from a scaling analysis and, as such, gives only an order of magnitude. This result can be easily extended to NI1, NI2, NI3, and the

multilayer experiments of Huang (1987) by considering only the wind-forced layers.

5. The inertial case

As pointed out in a review article by Ierley (1990), neglect of the inertial terms may be justified not only in the Sverdrup interior but also for the cross-shore component of the momentum equation in the vicinity of the Gulf Stream (semigeostrophic approximation). The difficulty comes in attempting to integrate this equation through the recirculation zone, which must inevitably be intersected in a zonal integration from the eastern boundary to the detached current. It is highly probable that the nonlinear terms there become important. As shown in section 4, neglect of the inertial terms in multilayer studies also leads to an upper-layer flow pattern dictated by the Sverdrup relation. Presumably, this dependence should disappear as soon as the inertial terms are included in the momentum equations. In this section, the effect of inertia on the experiments NI1, NI2, and NI3 of section 4a is investigated in detail.

a. Description of the time-averaged fields

Except for the presence of inertial terms in the momentum equations, experiments I1, I2, and I3 (Table 1) are identical to NI1, NI2, and NI3. Their time averaged upper-layer thicknesses and streamfunctions are presented in Fig. 7. As the amount of upper-layer fluid is reduced from I1 to I3 (λ = 0.19, 0.65, and 20.4, respectively) (Table 1), the outcrop region increases in size until it occupies more than half the domain in I3 (Fig. 7). As in section 4, the layer thicknesses were chosen such that the first two internal Rossby radii of deformation remain approximately constant. As in NI1 and NI2, only one layer outcrops in I1 and I2, while, as in NI3, three out of six layers outcrop in I3. This is illustrated by the two meridional vertical cross sections drawn respectively at 100 and 700 km east of the western boundary (Fig. 8). The separation latitude of the midlatitude jet is defined as the latitude at which the vorticity at the western wall changes sign, which also corresponds to the zero streamfunction line (Cessi 1991).

In I1 (Table 1), the second layer is observed to outcrop at the center of the subpolar gyre (Fig. 7a), and the separation latitude of the midlatitude jet is located 180 km south of the ZWCL (Table 2) (Fig. 7b). In this experiment, the outcrop region is very small and the upper layer covers most of the basin. By removing half the mass from the top layer (expt. I2, see Table 1), the outcrop area expands significantly and now covers most of the subpolar basin (Fig. 7c). As shown in Fig. 7d, the midlatitude jet separation latitude is moved further south (300 km south of the ZWCL, see Table 2). Remnants of the upper layer still circulate counterclockwise in the northern half of the basin (Fig. 7d). A further decrease of the initial layer thickness to 50 m in I3 reverses this trend of a southward movement of the jet separation latitude. The outcrop region covers more than half the basin (Fig. 7e), there is no more upper-layer circulation in the northern half of the domain and the jet separation latitude is now only 125 km south of the ZWCL (Table 2, Fig. 7f).

In each case, the jet separation is associated with a strong gradient in the isopycnal interface depths (Figs. 8a,c,e). Furthermore, this gradient is present at all interfaces and is aligned in the vertical, indicating a strong signature of the jet in all layers except the bottom one. This is confirmed by Figs. 9, 10, and 11, which display the streamfunctions of each layer for experiments I1, I2, and I3, respectively. In all three experiments, the midlatitude jet extends into the deeper layers and possesses a strong barotropic core underneath the recirculation region. The latter is consistent with Cessi's (1990) analytical results of a recirculation extending all the way to the bottom.

In the absence of outcropping (Chassignet and Gent 1991), the layers isolated from any forcing such as wind stress or bottom drag reveal large areas of well-homogenized potential vorticity (not illustrated) in agreement with the theory of Rhines and Young (1982). The question then arises as to whether potential vorticity homogenization occurs in the presence of outcropping. As illustrated in Figs. 12–14 for I1, I2, and I3, respectively, areas of homogenized potential vorticity are reduced in size in comparison to an experiment without outcropping and are confined to regions isolated from forcing, namely, the subtropical gyre where no layers outcrop (layer 3 of I1 in Fig. 12, layer 3 of I2 in Fig. 13, and layer 5 of I1 in Fig. 14, respectively).

The inertial experiments produce more intricate solutions than their noninertial counterparts. The Sverdrup relation no longer acts as a strong constraint on the upper-layer circulation, allowing the midlatitude jet separation point to move south of the ZWCL. As the amount of upper-layer fluid is reduced and the outcrop region increases, the jet separation latitude moves southward. This trend continues until all upper-layer fluid is evacuated from the subpolar gyre. Further reduction of upper-layer mass then appears to nudge the separation latitude northward back toward the ZWCL.

To be numerically stable, an experiment such as I3, with a small amount of upper-layer fluid, requires a larger eddy viscosity than experiment I2, which initially has a thicker upper layer. One might therefore attribute this reversal to a more viscous, that is, weaker, upper-layer circulation. To investigate this aspect, we performed an experiment (not illustrated) identical to I2, except that the eddy viscosity was chosen equal to that of I3 (Table 1). The separation latitude was observed to move northward by only 80 km versus the 175-km shift observed between I2 and I3 (Table 2). A larger viscosity is therefore not sufficient to account for the

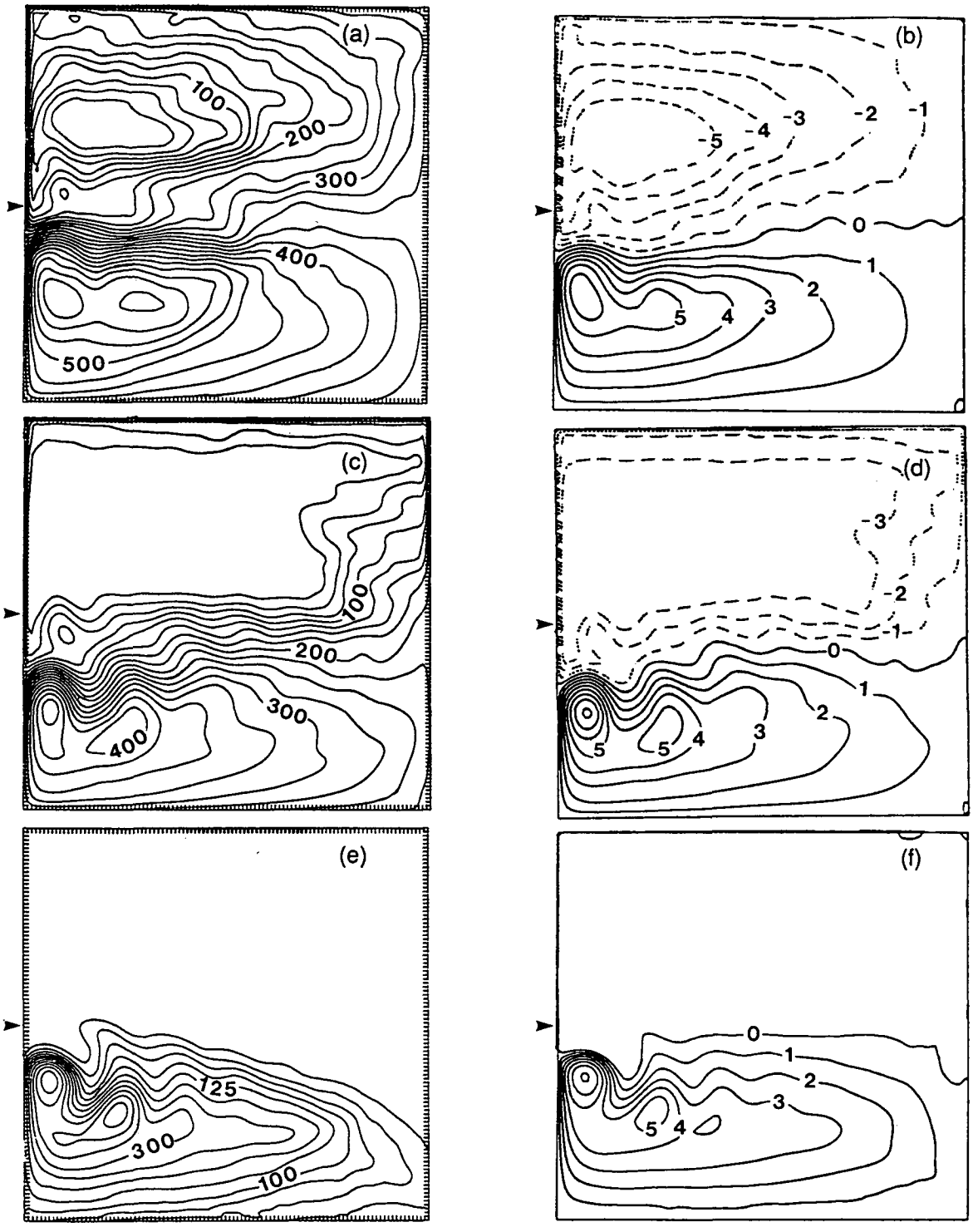

FIG. 7. As in Fig. 3 but for I1, I2, and I3, respectively.

observed reversal. Another explanation that can be advanced is that, as the circulation in the upper-layer subtropical gyre intensifies, the western boundary current overshoots its previous separation latitude (Cessi 1991).

b. Description of the instantaneous fields

The instantaneous flow patterns vary significantly as the outcrop region increases in size from I1 to I3. The upper-layer thickness fields at days 3520 and 3560

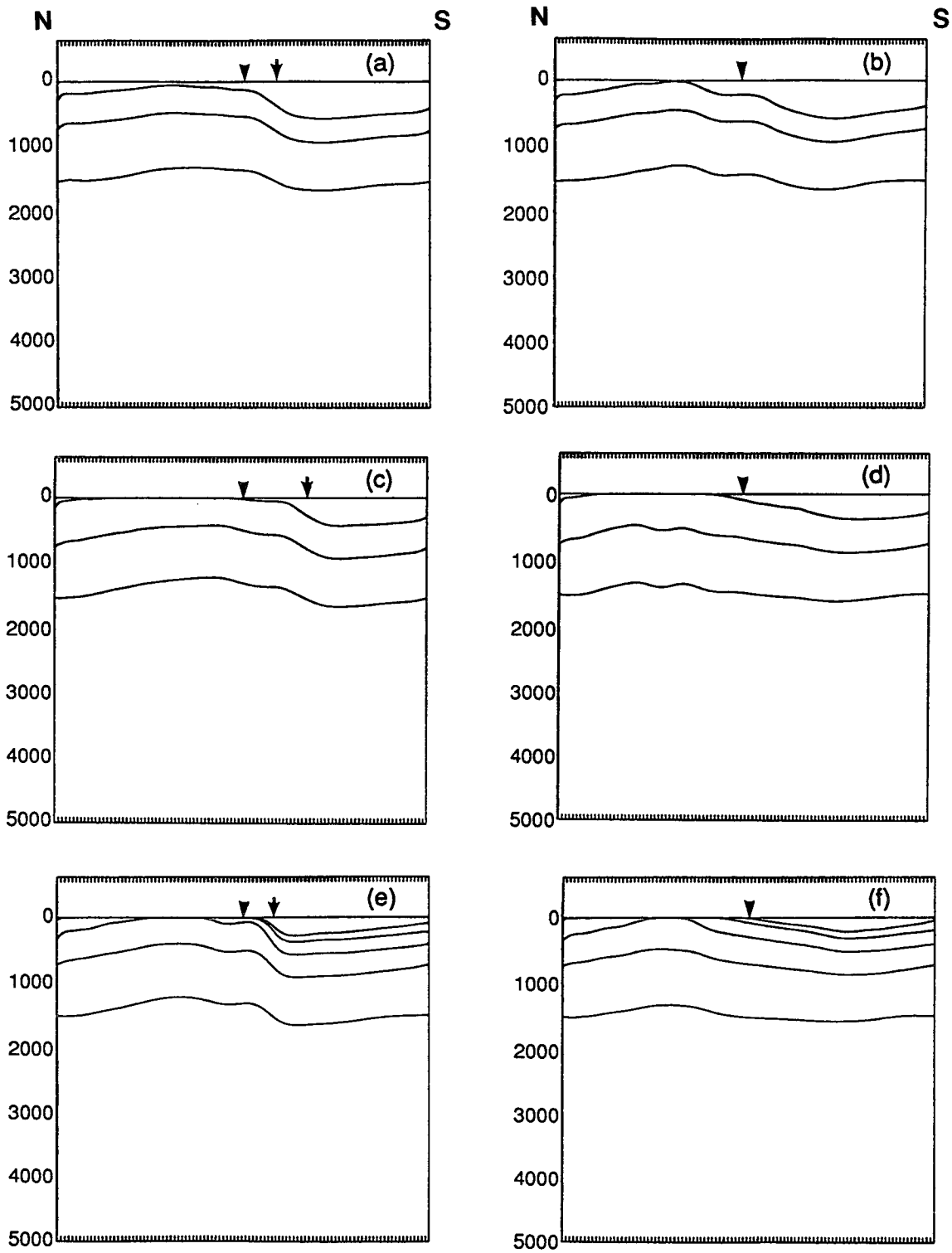

FIG. 8. As in Fig. 4 but for I1, I2, and I3, respectively. In (a), (c), and (e) the left arrow indicates the ZWCL and the right arrow, the midlatitude jet separation location.

of the 10-year integrations are displayed in Fig. 15 for the three experiments. In the case of a small outcrop area (Fig. 15a,b), the midlatitude jet extends quite far into the interior and both cyclonic and anticyclonic rings form through meander cutoff (Chassignet 1992). As the initial upper-layer thickness decreases in I2, λ

TABLE 2. Midlatitude jet separation location as a deviation from the *ZWCL* for I1, I2, and I3.

Experiment	Mean separation location (km)	d_{max} (m) when applicable
I1	180	
I2	300	
	230	500
I3	125	
	160	150
	125	500

and the global upper-layer Rossby number $\mathrm{Ro} = \tau_m / H_1 \beta^2 L^3$ increase, resulting in a larger outcrop area and a more intense upper-layer circulation, respectively (Fig. 15). Consequently, the midlatitude jet becomes more unstable, forms vigorous meanders, and is therefore less able to penetrate into the interior (Holland and Schmitz 1985; Barnier et al. 1991; Chassignet 1992) (Fig. 15c,d,e,f). Dissipation of potential vorticity is then accomplished through a vigorous anticyclonic recirculation gyre, which develops near the western boundary (Cessi et al. 1987; Cessi 1990).

In I2, the outcrop area does not completely cover the northern half of the basin, thereby providing space between the outcropping line and the midlatitude jet for anticyclonic rings to form and propagate westward (Fig. 15c,d). On the other hand, the outcropping line in I3 is associated with the midlatitude jet and anticyclonic ring formation is therefore inhibited (Figs. 15e,f). The question then arises as to whether anti-

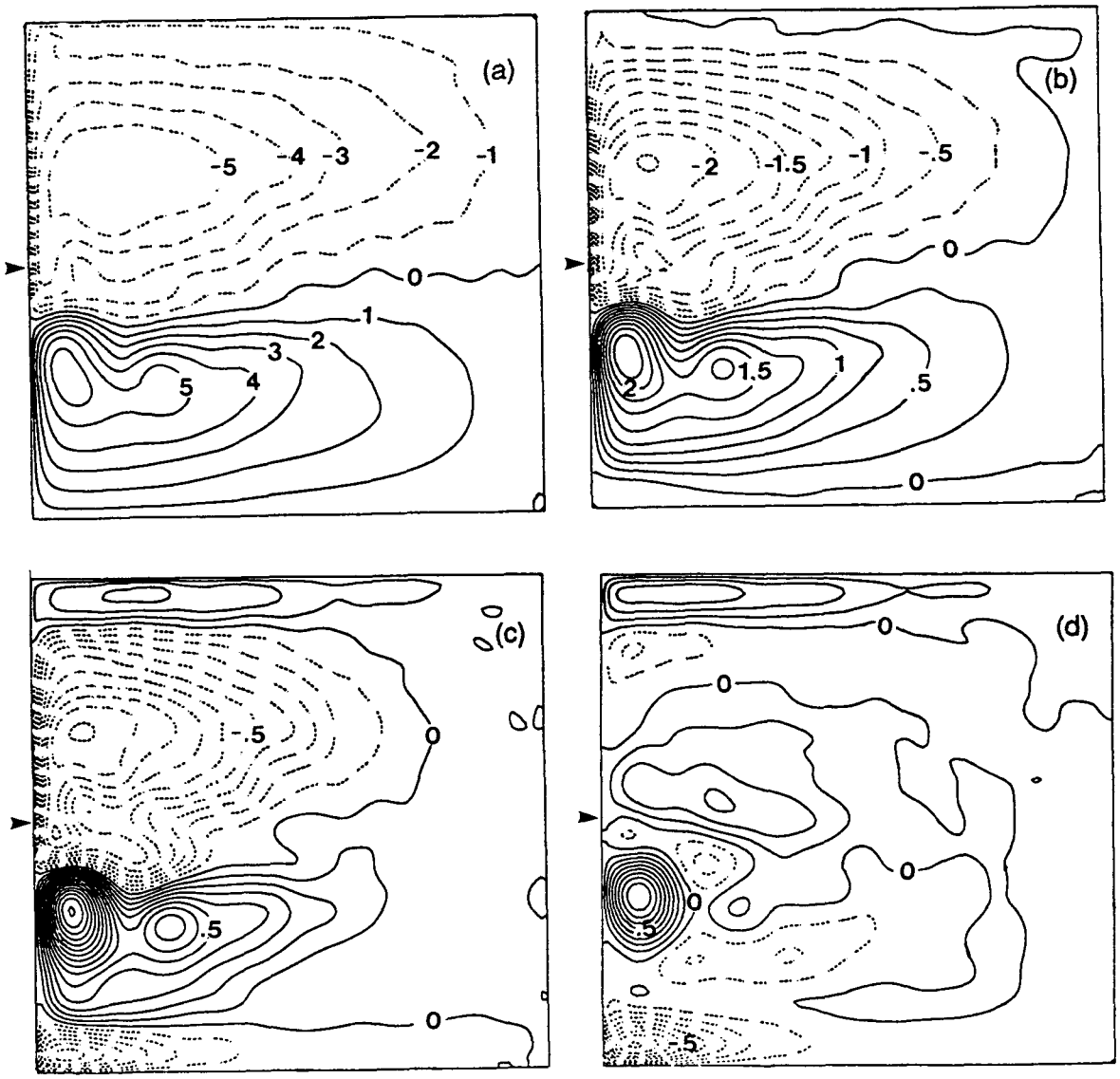

FIG. 9. Five-year time average velocity streamfunctions for each layer of I1. The contour intervals are 10^4 m^2 s^{-1} for (a), 2.5×10^3 m^2 s^{-1} for (b), and 10^3 m^2 s^{-1} for (c) and (d). The arrow indicates the ZWCL.

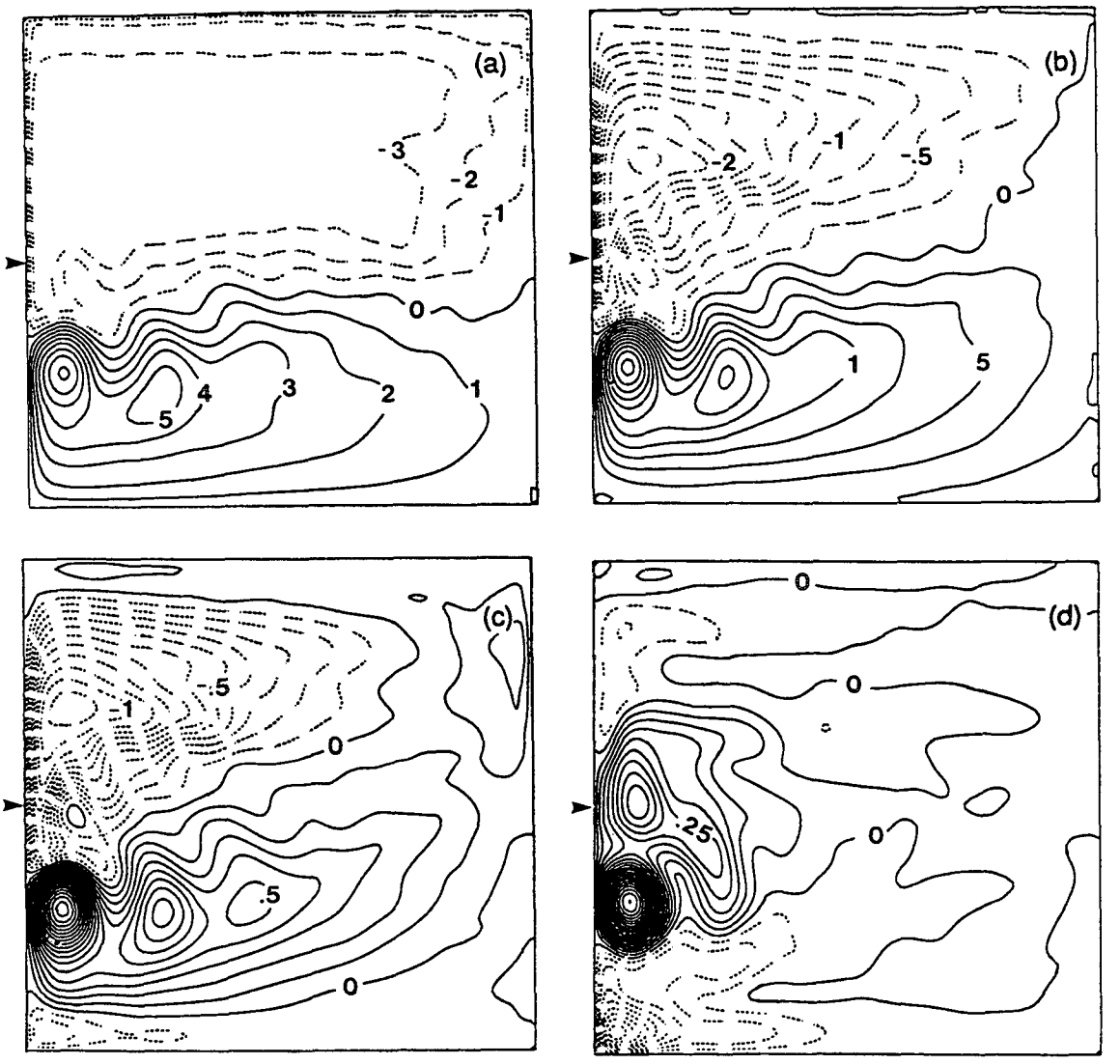

FIG. 10. As Fig. 9 for I2 except for (e) where the contour interval is 5×10^2 m^2 s^{-1}.

cyclonic rings can form in the lower layers underneath the outcrop associated with the midlatitude jet. The flow is quite coherent vertically; this results in instantaneous flow patterns of the lower layers (not illustrated) reproducing the upper circulation and consequently, no anticyclonic rings. On the other hand, cyclonic rings can form easily in both I2 and I3, but they tend to be reabsorbed quickly by the midlatitude jet.

c. *Importance of the choices in stratification and wind-forcing formulation*

The flow patterns discussed in sections 4 and 5 are strongly dependent upon the choice in initial upper-layer thickness despite the fact that the initial vertical discretization was performed to yield approximately the same first and second Rossby radii of deformation. In the experiments of section 4 and 5 as well as in Huang (1984, 1987), the wind forcing was defined as a body force acting *only* on the layer directly beneath the surface. This formulation is a function of the upper stratification and is likely to impact the resulting circulation. Furthermore, wind stress begins to act on a layer the moment it outcrops; this creates abrupt changes and temporal as well as spatial discontinuities in the layer circulation. While such a formulation has the advantage of leading to simple analytical solutions (section 3), the model's response becomes highly sensitive to the initial choices in stratification as illustrated by the results of sections 4 and 5a,b.

It is more realistic to assume that the depth over which the wind acts is related to the depth of a surface mixed layer. In the absence of mixed-layer dynamics, a discontinuity in the forcing can be avoided by defining a wind-stress profile that decreases from a value τ_0 at the surface to zero at some specified depth $d_{\max}$

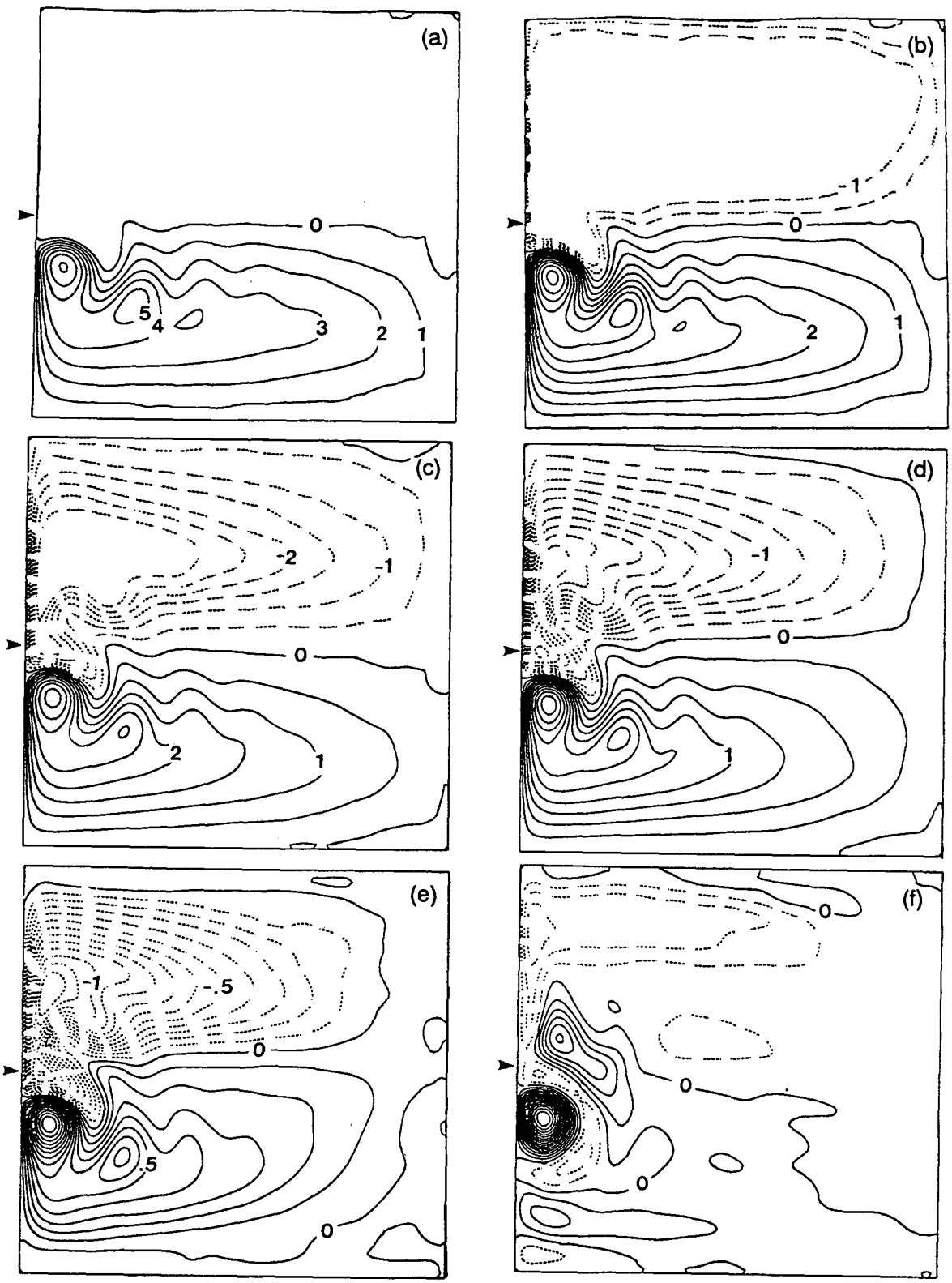

FIG. 11. Five-year time-averaged velocity streamfunctions for each layer of I3. The contour intervals are 10^4 m^2 s^{-1} for (a), 5×10^3 m^2 s^{-1} for (b) and (c), 2.5×10^3 m^2 s^{-1} for (d), and 10^3 m^2 s^{-1} for (e) and (f). The arrow indicates the ZWCL.

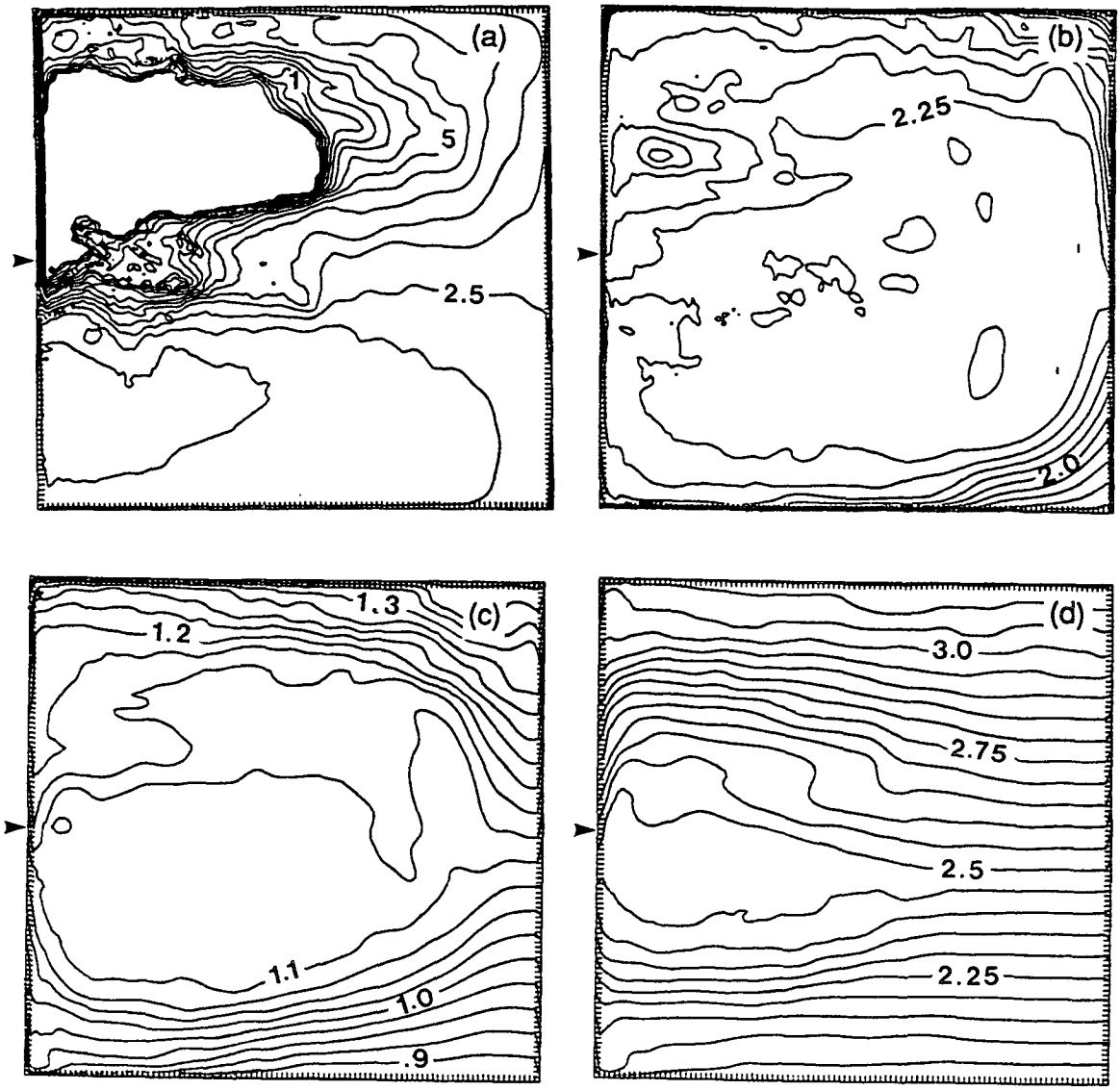

FIG. 12. Five-year time-averaged potential vorticity for each layer of I1. The contour intervals are 10^{-12} m^{-1} s^{-1} for (a), (b), and (c), and 10^{-13} m^{-1} s^{-1} for (d). The contours higher than 10^{-6} m^{-1} s^{-1} are not shown and the arrow indicates the ZWCL.

(Bleck and Boudra 1986). The number of layers over which the wind acts is then likely to vary with time and location depending upon the number of layers encountered within d_{max}. In the case of a linear profile, the wind stress is given by $\tau = \tau_0[1 - (d/d_{max})]$. The force acting on layer k can then be expressed as

$$\frac{\tau_0}{d_{max}}\left(\frac{\min(d_k, d_{max}) - \min(d_{k-1}, d_{max})}{d_k - d_{k-1}}\right), \quad (5)$$

where d_k is the corresponding lower interface depth ($d_0 = 0$). This formulation is such that the total Sverdrup transport is conserved.

In cases where the first interface depth d_1 is always greater than d_{max}, (5) yields the traditional body force τ_0/d_1. If d_1 becomes smaller than d_{max}, the upper layer will continue to be accelerated by τ_0/d_{max} while the second layer, providing that the second interface is deeper than d_{max}, will experience an acceleration

$$\frac{\tau_0}{d_{max}}\frac{(d_{max} - d_1)}{d_2 - d_1}.$$

Similar expressions can be derived from (5) when several layers are within d_{max}. Such a formulation provides a smooth transition in wind forcing as layers outcrop. Its impact on the model response is now investigated for the two inertial experiments with large outcrop areas, namely I2 and I3.

Because of the coarse vertical discretization, d_{max} has to be chosen deep enough to include several layers in order for the resulting circulation to differ. For exper-

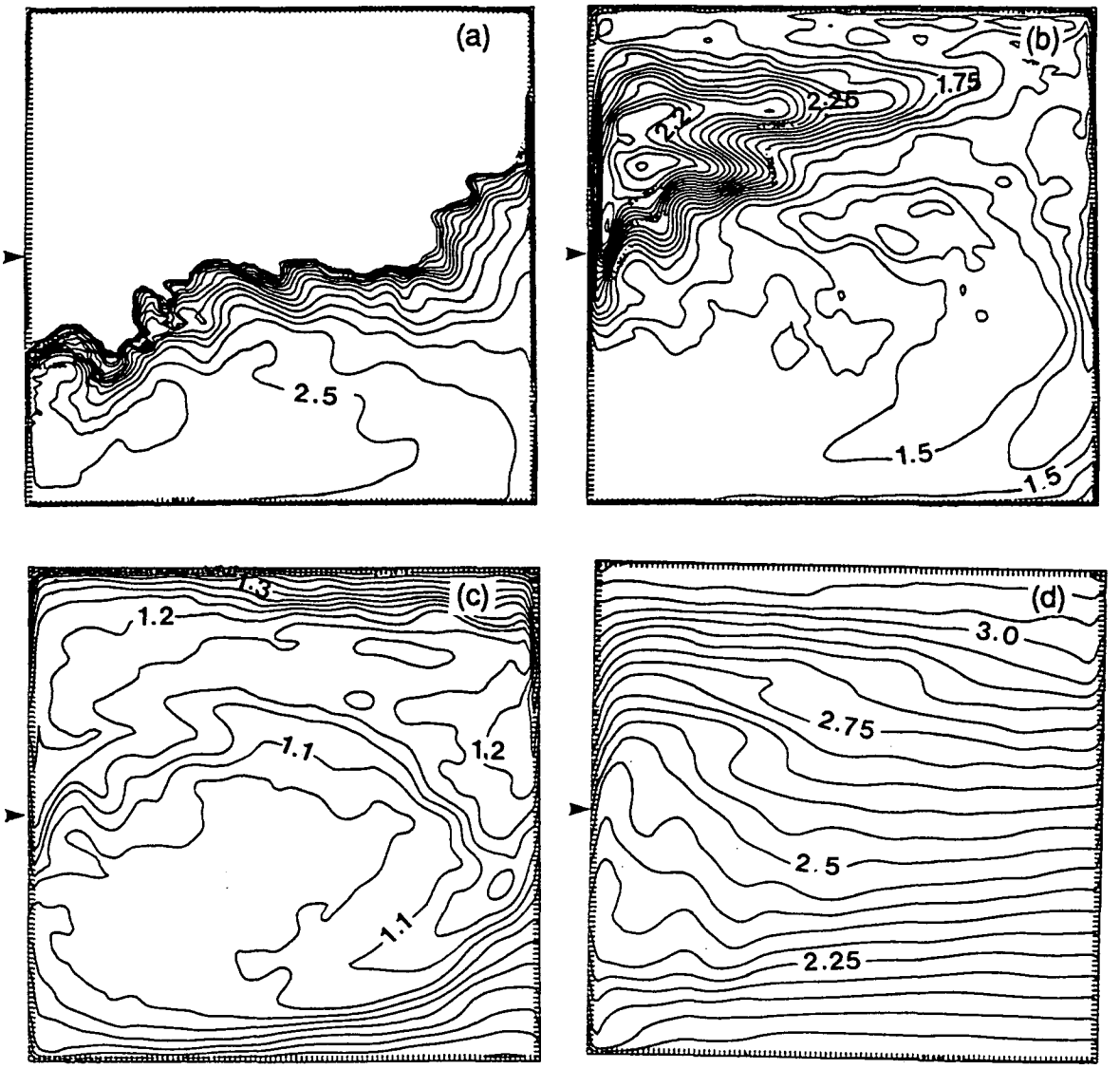

FIG. 13. As in Fig. 12 but for I2.

iment I2, only one case (d_{max} = 500 m) is discussed while for I3, because of its higher vertical resolution in the upper 500 m, two cases (d_{max} = 150 and 500 m) are presented. The time-averaged upper-layer streamfunction with the different d_{max} for both I2 and I3 are displayed in Fig. 16. In comparison with the experiment presented in section 5a, the outcrop area of I3 with d_{max} = 150 m (Fig. 16a) increased in size and the midlatitude jet separation latitude moved south by 35 km (Table 2). This is in agreement with the findings of section 5a since the upper-layer circulation is now less intense. Further weakening of the upper-layer circulation is achieved with a deeper d_{max} (Fig. 16b). The resulting outcrop area is then considerably reduced in size and the separation latitude moves back toward the ZWCL (Table 2). The circulation is now less inertial and the midlatitude jet extends further into the interior. Both anticyclonic and cyclonic rings are able to form. A similar result is obtained for I2 with a d_{max} of 500 m (Fig. 16c). The outcrop area is also reduced considerably in size, the circulation is less intense and the separation latitude moved back toward the ZWCL by 70 km (Table 2). The circulations in I2 and I3 with d_{max} = 500 m, if not identical, are at least in much closer agreement than the experiments of section 5a driven by the simple assumption of a wind forcing acting only on the layer in direct contact with the wind.

6. Summary and concluding remarks

The experiments described in this paper were aimed at developing an understanding of the jet separation in large-scale eddy-resolving simulations since most realistic experiments to date have a midlatitude jet

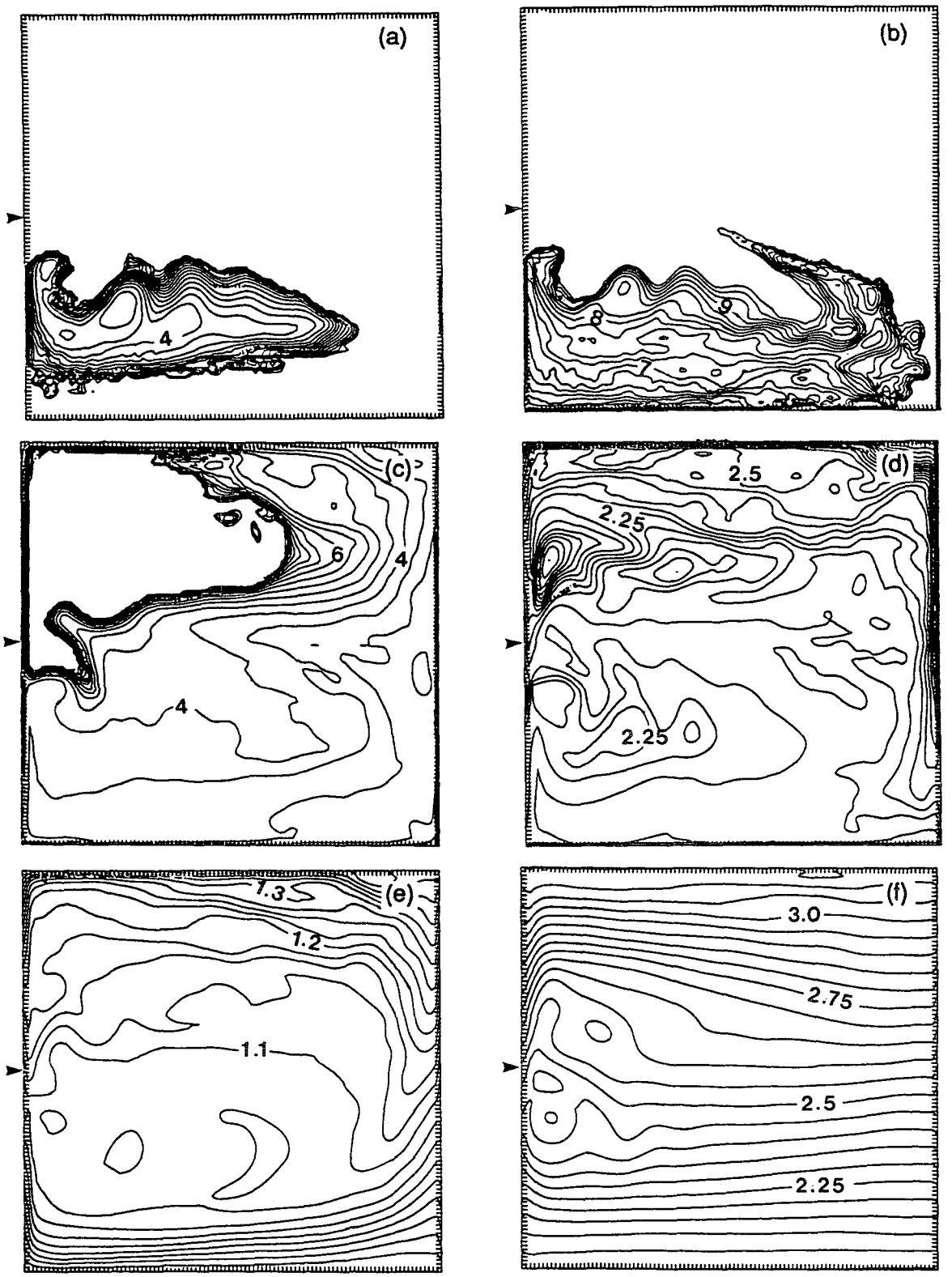

FIG. 14. Five-year time-averaged potential vorticity for each layer of I3. The contour intervals are 10^{-12} m^{-1} s^{-1} for (a), (b), (c), (d), and (e), and 10^{-13} m^{-1} s^{-1} for (f). The contours higher than 10^{-6} m^{-1} s^{-1} are not shown and the arrow indicates the ZWCL.

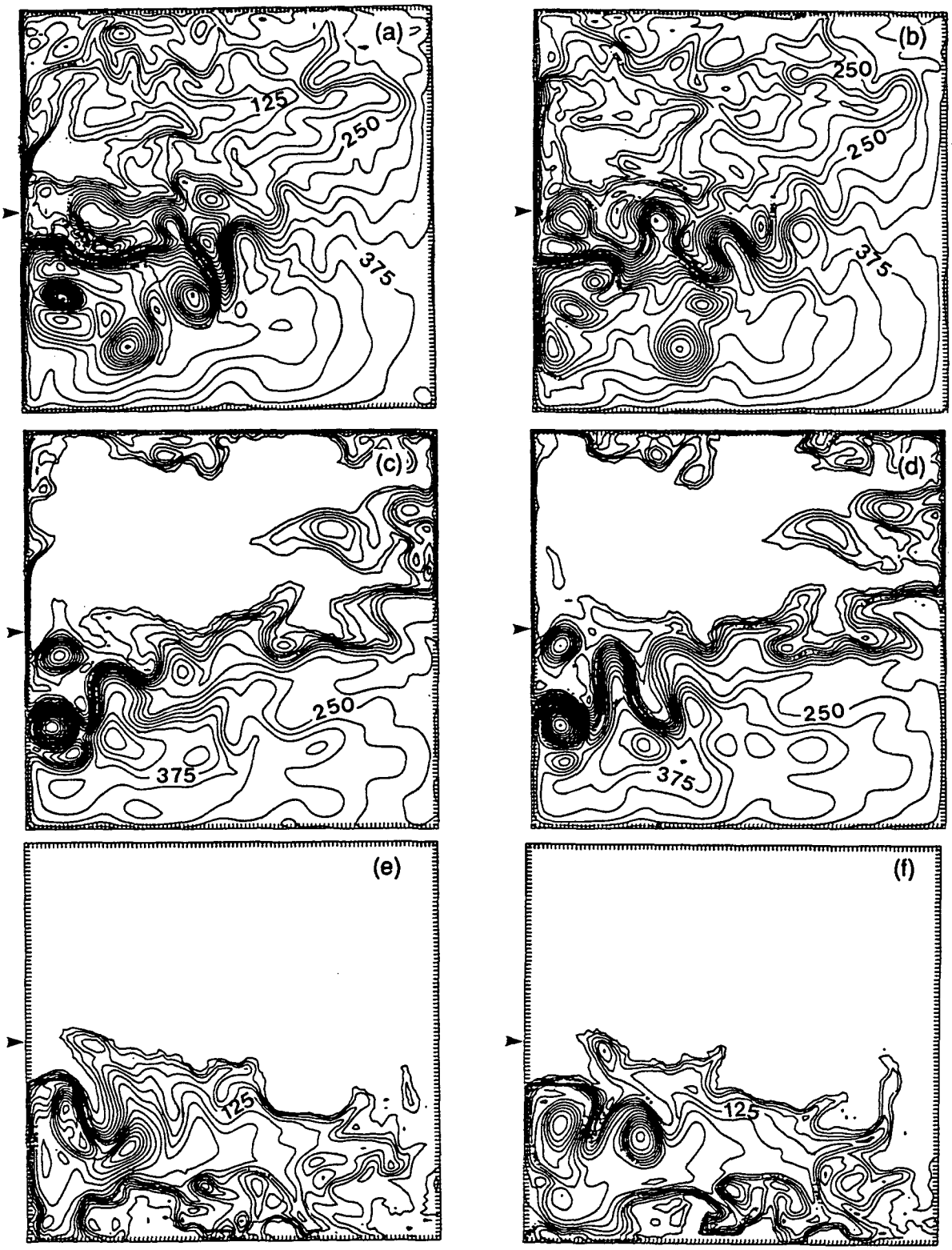

FIG. 15. Instantaneous upper-layer thickness fields at days 3520 and 3560 for I1, I2, and I3, respectively. The contour intervals are 25 m and the arrow indicates the ZWCL.

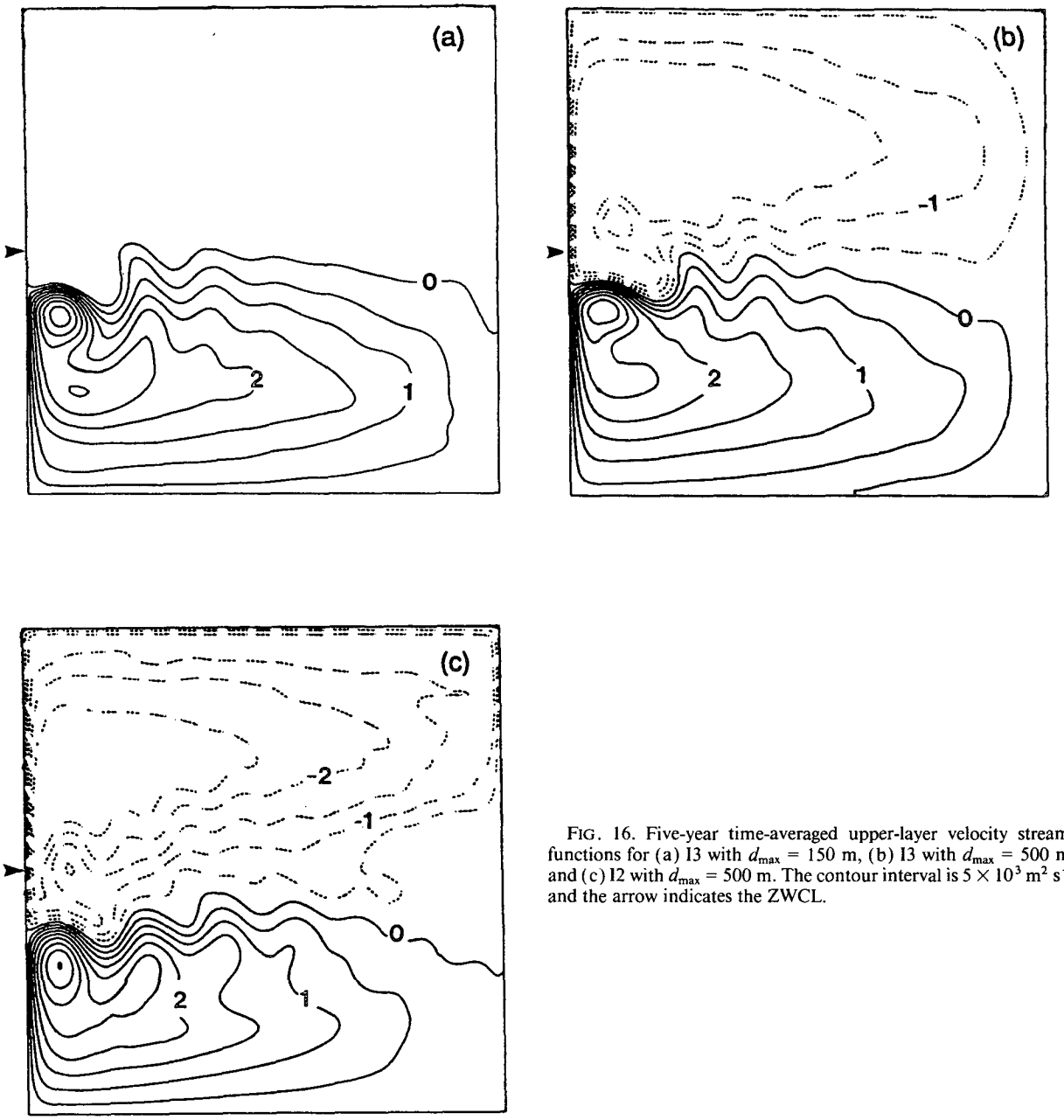

FIG. 16. Five-year time-averaged upper-layer velocity streamfunctions for (a) I3 with d_{max} = 150 m, (b) I3 with d_{max} = 500 m, and (c) I2 with d_{max} = 500 m. The contour interval is 5×10^3 m^2 s^{-1} and the arrow indicates the ZWCL.

that overshoots the ZWCL (Thompson and Schmitz 1989; Chassignet and Gent 1991). The influence of outcropping on midlatitude jet separation was therefore investigated in a series of purely wind-driven eddy-resolving primitive equation numerical experiments of increasing complexity. On one hand, the outcropping mechanism of Parsons (1969) allows the midlatitude jet to separate south of the ZWCL, while, on the other, the separation latitude depends upon the stratification choices and upon the assumption of a fixed amount of fluid in the layers. When only the nonlinearity associated with layer depth changes is taken into account, that is, no inertial terms in the momentum equations, the Sverdrup relation $\beta V = \text{curl}\tau$ dictates the resulting upper-layer flow pattern. As long as the upper/lower-layer ratio δ is small enough, the two-layer numerical experiments agree with the analytical theory and both the outcropping line and the upper-layer midlatitude jet separation latitude are located south of the zero wind stress curl line. A baroclinic exchange of mass across the ZWCL is then necessary to satisfy the Sverdrup relation in the interior. In the case of a large δ, the flow pattern changes drastically and the midlatitude jet separation point shifts to the ZWCL. The resulting

circulation then favors a pattern that satisfies the Sverdrup relation with no baroclinic exchange of mass across the ZWCL. This result can be easily extended to multilayer cases by considering only the wind-forced layers.

The constraint imposed by the Sverdrup relation on the upper-layer circulation disappears as soon as the inertial terms are included in the momentum equations. As the amount of upper-layer fluid is reduced, the outcrop region increases in size and the midlatitude jet separation latitude moves south of the ZWCL. This trend is reversed when the distribution of water masses in the upper layer is such that the circulation in the subpolar gyre vanishes. The separation latitude then moves northward back toward the ZWCL. In these experiments, the resulting circulation is highly sensitive to the stratification choices since the wind forcing is prescribed as a body force acting only on the layer in direct contact with the atmosphere. Temporal and spatial discontinuities in forcing then appear as layers outcrop. This discrete forcing mode can be avoided by adopting a formulation that provides a gradual transition in wind forcing as layers outcrop. If the wind stress is assumed to decrease from a maximum at the surface to zero at some specified depth, the flow patterns from experiments with different initial stratification agree much more closely with each other than they do if only the topmost layer is being forced.

In the ocean, the depth over which the wind acts is time and space dependent and is usually assumed to be the depth of the mixed layer. In the absence of thermodynamics in the model, the amount of fluid in the upper layer is fixed and this amount, together with the wind-forcing formulation, dictates the outcrop location and size. However, as discussed by Pedlosky (1987b) and Nurser and Williams (1990), the presence of cross-isopycnal flows at the outcrop of the thermocline may affect the nature of the solution. If a moderate mass conversion is permitted (i.e., a "leaky" Ekman-layer flow), Pedlosky (1987b) argued that the outcrop of the thermocline might no longer be associated with a detached boundary current. Nurser and Williams (1990) actually showed that artificial heating along the outcrop line weakens the separating boundary current and shifts its path northward. They showed Pedlosky's solution to be a special limit of maximum possible heating. On the other hand, realistic cooling resulted in a strengthening of the boundary current and in a southward shift of its separation point. This raises the question to what extent the midlatitude jet separation mechanism in the presence of outcropping layers is modified by the presence of a thermodynamically active mixed layer. In part II of this paper, the influence of a mixed layer on the midlatitude jet separation will be investigated by merging a thermodynamically active Kraus–Turner-type mixed layer to the numerical model used in this paper (Bleck et al. 1989). An additional advantage of adding a mixed layer is that the ambiguities associated with distributing the wind forcing over various layers are removed. Other diabatic effects such as deep-water formation and diapycnal mixing are also likely to have an impact on the midlatitude jet separation.

Finally, separation mechanisms other than outcropping layers have been proposed in the literature, such as separation by "vorticity crisis" (Pedlosky 1987a, Verron and LeProvost 1991) or by "adverse pressure gradient" (Cessi 1991; Haidvogel et al. 1992). These mechanisms are, however, sensitive to the choices of lateral boundary conditions (Haidvogel et al. 1992). For example, in the latter work, the choice of no-slip lateral boundary conditions leads to an early separation of the midlatitude jet and the formation of a double Gulf Stream. In contrast, the outcropping mechanism discussed in this paper, being a large-scale response, is in principle independent of the choice made for the lateral boundary condition.

Acknowledgments. Discussions with B. Cushman-Roisin, W. Dewar, R. Salmon, and especially G. Veronis proved timely and valuable. Support was provided by the National Science Foundation through Grant OCE-9102560. Computations were carried out using the CRAY Y-MP at the National Center for Atmospheric Research (NCAR). NCAR is sponsored by the National Science Foundation.

REFERENCES

Anderson, D. L. T., and P. D. Killworth, 1979: Nonlinear propagation of long Rossby waves. *Deep-Sea Res.*, **26**, 1033–1050.

——, and D. W. Moore, 1979: Cross-equatorial inertial jets with special relevance to very remote forcing of the Somali Current. *Deep-Sea Res.*, **26A**, 1–22.

Barnier, B., B. L. Hua, and C. Le Provost, 1991: On the catalytic role of high baroclinic modes in eddy-driven large-scale circulation. *J. Phys. Oceanogr.*, **21**, 976–997.

Bleck, R., and D. B. Boudra, 1981: Initial testing of a numerical ocean circulation model using a hybrid (quasi-isopycnic) vertical coordinate. *J. Phys. Oceanogr.*, **11**, 755–770.

——, and ——, 1986: Wind-driven spin up in eddy-resolving ocean models formulated in isopycnic and isobaric coordinates. *J. Geophys. Res.*, **91**, 7611–7621.

——, and L. T. Smith, 1990: A wind-driven isopycnic coordinate model of the North and Equatorial Atlantic Ocean. Part I: Model development and supporting experiments. *J. Geophys. Res.*, **95**, 3273–3285.

——, H. P. Hanson, D. Hu, and E. B. Kraus, 1989: Mixed layer/thermocline interaction in a three-dimensional isopycnal model. *J. Phys. Oceanogr.*, **19**, 1417–1439.

Bogue, N. M., R. X. Huang, and K. Bryan, 1986: Verification experiments with an isopycnal coordinate ocean model. *J. Phys. Oceanogr.*, **16**, 985–990.

Boris, J. P., and D. L. Book, 1973: Flux-corrected transport. I: SHASTA, A fluid transport algorithm that works. *J. Comput. Phys.*, **11**, 38–69.

Bryan, K., 1963: A numerical investigation of a nonlinear model of a wind-driven ocean. *J. Atmos. Sci.*, **20**, 594–606.

Cessi, P., 1990: Recirculation and separation of boundary currents. *J. Mar. Res.*, **48**, 1–35.

——, 1991: Laminar separation of colliding western boundary currents. *J. Mar. Res.*, **49**, 697–717.

——, G. R. Ierley, and W. R. Young, 1987: A model of inertial recirculation driven by potential vorticity anomalies. *J. Phys. Oceanogr.*, **17**, 1640–1652.

——, R. V. Condie, and W. R. Young, 1990: Dissipative dynamics of western boundary currents. *J. Mar. Res.*, **48**, 677–700.

Chassignet, E. P., 1992: Rings in numerical models of ocean general circulation: A statistical study. *J. Geophys. Res.*, **97,** 9479–9492.
——, and B. Cushman-Roisin, 1991: On the influence of a lower layer on the propagation of nonlinear oceanic eddies. *J. Phys. Oceanogr.*, **21,** 939–957.
——, and P. R. Gent, 1991: The influence of boundary conditions on midlatitude jet separation in ocean numerical models. *J. Phys. Oceanogr.*, **21,** 1290–1299.
Colin de Verdière, A., 1986: On mean flow instabilities within the planetary geostrophic equations. *J. Phys. Oceanogr.*, **16,** 1981–1984.
Dewar, W. K., 1987: Planetary shock waves. *J. Phys. Oceanogr.*, **17,** 470–482.
——, 1991: Arrested fronts. *J. Mar. Res.*, **49,** 21–52.
Haidvogel, D. B., J. L. Wilkin, and R. Young, 1991: A semi-spectral primitive equation ocean circulation model using vertical sigma and orthogonal curvilinear horizontal coordinates. *J. Comput. Phys.*, **94,** 151–185.
——, J. C. McWilliams, and P. R. Gent, 1992: Boundary current separation in a quasigeostrophic, eddy-resolving ocean circulation model. *J. Phys. Oceanogr.*, **22,** 882–902.
Holland, W. R., 1978: The role of mesoscale eddies in the general circulation of the ocean—Numerical experiments using a wind-driven quasigeostrophic model. *J. Phys. Oceanogr.*, **8,** 363–392. 392.
——, and L. B. Lin, 1975: On the generation of mesoscale eddies and their contribution to the oceanic general circulation. Parts I and II. *J. Phys. Oceanogr.*, **5,** 642–669.
——, and W. J. Schmitz, 1985: Zonal penetration scale of model midlatitude jets. *J. Phys. Oceanogr.*, **15,** 1859–1875.
Huang, R. X., 1984: The thermocline and current structure in subtropical/subpolar basins. Ph.D. thesis, Massachusetts Institute of Technology WHOI-84-42, 218 pp.
——, 1986: Numerical simulation of wind-driven circulation in a subtropical/subpolar basin. *J. Phys. Oceanogr.*, **16,** 1636–1650.
——, 1987: A three-layer model for wind-driven circulation in a subtropical-subpolar basin. Part I: Model formulation and the subcritical state. Part II: The supercritical and hypercritical states. *J. Phys. Oceanogr.*, **17,** 664–678; 679–697.
——, and K. Bryan, 1987: A multilayer model of the thermocline and wind-driven ocean circulation. *J. Phys. Oceanogr.*, **17,** 1909–1924.
——, and G. Flierl, 1987: Two-layer models for the thermocline and current structure in subtropical/subpolar gyres. *J. Phys. Oceanogr.*, **17,** 872–884.
Ierley, G. R., 1990: Boundary layers in the general ocean circulation. *Annu. Rev. Fluid. Mech.*, **22,** 111–142.
Kamenkovich, V. M., and G. M. Reznik, 1972: A contribution to the theory of stationary wind-driven currents in a two-layer liquid. *Izv. Acad. Sci. USSR, Atmos. Ocean. Phys.* [English Translation], **8,** 238–245.
McWilliams, J. C., N. J. Norton, P. R. Gent, and D. B. Haidvogel, 1990: A linear balance model of wind-driven, midlatitude ocean circulation. *J. Phys. Oceanogr.*, **20,** 1349–1378.
Moore, D. W., and P. P. Niiler, 1974: A two-layer model for the separation of inertial boundary currents. *J. Mar. Res.*, **32,** 457–484.
Nurser, A. J. G., and R. G. Williams, 1990: Cooling Parsons's model of the separated Gulf Stream. *J. Phys. Oceanogr.*, **20,** 1974–1979.
Ou, H. W., and W. P. M. de Ruijter, 1986: Separation of an inertial boundary current from a curved coastline. *J. Phys. Oceanogr.*, **16,** 280–289.
Parsons, A. T., 1969: A two-layer model of Gulf Stream separation. *J. Fluid Mech.*, **39,** 511–528.
Pedlosky, J., 1987a: *Geophysical Fluid Dynamics.* 2d ed. Springer-Verlag, 624 pp.
——, 1987b: On Parsons' model of the ocean circulation. *J. Phys. Oceanogr.*, **17,** 1571–1582.
Phillips, N. A., 1954: Energy transformations and meridional circulations associated with simple baroclinic waves in a two-level, quasigeostrophic model. *Tellus,* **6,** 273–286.
Rhines, P. B., 1986: Vorticity dynamics of the oceanic general circulation. *Annu. Rev. Fluid Mech.*, **18,** 433–497.
——, and W. R. Young, 1982: A theory of the wind-driven circulation. Part I: Midocean gyres. *J. Mar. Res.*, **40,** 559–596.
Smith, L. T., D. B. Boudra, and R. Bleck, 1990: A wind-driven isopycnic coordinate model of the North and Equatorial Atlantic Ocean. 2: The Atlantic basin experiments. *J. Geophys. Res.*, **95,** 13 105–13 128.
Thompson, J. D., and W. J. Schmitz, 1989: A limited-area model of the Gulf Stream: Design, initial experiments, and model-data intercomparison. *J. Phys. Oceanogr.*, **19,** 791–814.
Veronis, G., 1973: Model of world ocean circulation: I. Wind-driven, two-layer. *J. Mar. Res.*, **31,** 228–288.
——, 1981: Dynamics of large-scale ocean circulation. *Evolution of Physical Oceanography,* B. A. Warren and C. Wunsch, Eds., The MIT Press, 140–183.
Verron, J., and C. LeProvost, 1991: Response of eddy-resolved general circulation models to asymmetrical wind forcing. *Dyn. Atmos. Oceans,* **15,** 505–533.
Welander, P., 1966: A two-layer frictional model of wind-driven motion in a rectangular oceanic basin. *Tellus,* **18,** 54–62.
Zalesak, S. T., 1979: Fully multidimensional flux-corrected transport algorithms for fluids. *J. Comput. Phys.*, **31,** 335–362.